Effects of off-diagonal radiative-decay coupling on electron transitions in resonant double quantum wells

Danhong Huang and D. A. Cardimona
Air Force Research Laboratory (AFRL/VSSS), 3550 Absentee Avenue SE, Building 426, Kirtland Air Force Base, New Mexico 87117
(Received 18 December 2000; revised manuscript received 21 March 2001; published 18 June 2001)

Density-matrix equations for electrons in laser-coupled quantum wells are derived in second quantization, including an off-diagonal radiative-decay coupling between a pair of electron transitions. Calculations of spontaneous photoluminescence and time-resolved optical absorption for the probe field are formulated. The zero absorption of the pump-laser field within an overlapping region between two absorption peaks is found in a resonant asymmetric double-quantum-well system and explained as the quantum interference between two nearly degenerate electron transitions. Quantum interference is clearly demonstrated through phase cancellation between the two statistically averaged transition dipole moments. The laser frequency for zero absorption can be tuned within a tunneling gap by applying a small dc bias field. The $k_{\|}$-dependent energy-level separation is found to be a crucial factor for destroying quantum interference. The optical gain of the probe field is seen as a hole in the weak absorption peak for the resonant asymmetric double quantum wells selectively coupled by a laser field and shown to be a result of the partial inversion of the electron occupation probabilities in momentum space after laser excitation. The probe-field gain increases with the strength of the pump laser. The effects of transition blocking, induced quantum coherence, and off-diagonal radiative-decay coupling are quantitatively analyzed for this gain.

DOI: 10.1103/PhysRevA.64.013822 PACS number(s): 42.50.Ct, 42.50.Hz, 42.50.Md

I. INTRODUCTION

When a laser is applied to resonantly excite a multilevel atomic system, there exists *quantum interference* in the absorption and emission spectra. A proper theory [1] for the radiative decay of excited electrons in an atomic system requires a quantum electrodynamic treatment of photons and electrons in second quantization. In addition to the usual diagonal radiative-decay time, there is an *off-diagonal radiative-decay coupling* (ODRDC) that becomes important when two or more electron transition energies are very close [2]. The effect of ODRDC describes a nearly resonant absorption of a spontaneously emitted photon from one downward electron transition by another upward electron transition. With the existence of ODRDC, any two nearly degenerate electron transitions that are excited by a pump laser and share a common initial state will be coupled and interfere with each other, giving rise to zero absorption [2–4] in the region between the two overlapping absorption peaks.

The recent proposals for electromagnetically induced transparency [5] and lasing without population inversion [6] in atomic gases, which utilize a concept similar to the above quantum interference, have attracted a lot of attention and have been confirmed experimentally [7,8]. For the sake of device applications, these interests have been directed from atomic gases to electron gases in semiconductor quantum wells (QW's). The schemes that are proposed for observing electromagnetically induced transparency in QW's include the Fano-type interference [9,10] and a pair of coherently prepared dressed states [11]. For observing lasing without population inversion in QW's, a number of proposals have been put forward by several research groups [12–14] to employ electron intersubband transitions within the conduction band of QW's.

However, an electron gas in QW's and atomic vapor differ in many ways. Here, we list some unique features of electron gases compared to those of atomic gases. First, an electron in an atom is bound by a rotationally invariant Coulomb potential due to the positively charged nucleus, but an electron in a QW is confined by a controllable one-dimensional quantum-well potential due to the conduction-band offset. Therefore, the selection rule for optical transitions of electrons in these two systems is quite different. Second, an electron in an atom experiences a three-dimensional strong confinement ($\sim$0.5 Å), but an electron with much smaller effective mass in a QW is only subjected to a one-dimensional weak confinement ($\sim$100 Å). Consequently, the energies of electron transitions in these two systems differ by two orders of magnitude. Third, the energy levels in an atom are flat in momentum space, but those in a QW are dispersive within the quantum-well plane. This leads to a momentum-dependent energy-level separation and electron scattering within the same subband in the QW's. Fourth, the energy levels of an electron in a QW can be engineered by choosing various materials for the well and barrier layers, or by adjusting the well thickness. Finally, there are only a few electrons in an atom that can interact, but there is a tremendous number of electrons in QW's. This results in many-body effects, i.e., the enhancement of the Coulomb energy of QW electrons compared to their kinetic energy. Moreover, there exist several additional scattering processes for electrons in QW's, including electron-electron, electron-phonon, electron-roughness, and electron-impurity scattering. In this paper, we will concentrate on some dominant new effects arising from these unique features of QW's.

Recently, Imamoğlu and Ram [13] proposed a double-quantum-well (DQW) structure for demonstrating the mechanism of lasing without inversion in semiconductors based on earlier work in an atomic system [15], in which the

laser pumping [15] between the two upper levels has been replaced by a coherent electron tunneling [13] between the two QW's. The selective excitation of electrons from the ground level to the top level 3 in the atomic system [15] can be easily realized since the two upper laser-coupled levels 2 and 3 are well separated in energy. However, the selective excitation of electrons localized only in the right QW [13] becomes extremely difficult experimentally due to the energy resonance between the levels 2 and 3 in the left and right QW's. In the current paper, the same DQW structure is considered, in which the coherent electron tunneling between the two QW's gives rise to a split doublet in the dressed-state picture. Moreover, a pump laser that excites the electrons from the ground level to the upper doublet is applied to the structure. The excitation of electrons in our model is not a selective one localized only in one of the two QW's but a nonselective one delocalized in both QW's. If both excitations of electrons from the ground level to the two upper degenerate levels 2 and 3 in the left and right QW's [13] are added together in the absence of the ODRDC, the resulting absorption spectrum will simply display an overlap of the two absorption peaks as indicated by the dashed curve in Fig. 2(b). There is no zero absorption within the gap region, although there exists coherence between the upper two resonant levels. For the nonselective excitation of electrons in DQW's, only when the ODRDC is introduced can the zero absorption of the pump laser within the tunneling gap and the amplification of another probe field be seen. As long as an upper nearly degenerate doublet exists in the system, the effect of ODRDC is intrinsic, which modifies the optical response of electrons in DQW's.

The organization of this paper is as follows. Section II is devoted to the second quantization of the electron Hamiltonian and the electromagnetic field, as well as the interaction between them. The equations of motion for electrons are derived by using many-particle ascending/descending operators in Sec. III, and the density-matrix equations are obtained in Sec. IV on the basis of the equations of motion. Using these density-matrix equations, we study two- and three-level models for QW's pumped by a laser in Sec. V, and present the formula for calculating the time-resolved absorption and photoluminescence spectra. Numerical results and discussions are given in Sec. VI for the laser-field absorption and refractive-index function in three-level resonant asymmetric double quantum wells (RADQWs), where the zero absorption within an overlapping region of two absorption peaks is found to be due to quantum interference between two nearly degenerate electron transitions. The probe-field absorption spectrum for this laser-coupled system is also presented in this section, where the optical gain is seen as a hole in the weak absorption peak, and the effects of induced quantum coherence and ODRDC on the optical gain are quantitatively analyzed. The paper is concluded in Sec. VII.

II. QUANTIZATION OF THE ELECTRON HAMILTONIAN AND AN ELECTROMAGNETIC FIELD

In this section, we first consider second quantization of the electron Hamiltonian using the electron annihilation/creation operators in the QW's, where the many-particle ascending/descending operators are introduced. After this, the quantization of an electromagnetic field is performed with the help of the photon annihilation/creation operators. Finally, the interaction between the electromagnetic field and electrons in the QW's is quantized by expressing it as a combination of electron and photon annihilation/creation operators.

A. Second quantization of the electron Hamiltonian in quantum wells

The first quantization of the electron Hamiltonian leads to the energy quantization determined by the single-electron Schrödinger equation in Eq. (A19). The fermion statistics in a many-electron system is still absent. In second quantization, however, the fermion statistics of indistinguishable electrons is employed to directly quantize the Hamiltonian of electrons in the QW's. Given any time-dependent electron field operator $\hat{\Psi}(\mathbf{r},t)$, we can expand it in momentum space as [16]

$$\hat{\Psi}(\mathbf{r},t)=\sum_{j,\mathbf{k}_\parallel}\hat{C}_{j\mathbf{k}_\parallel}(t)\psi_{j\mathbf{k}_\parallel}(\mathbf{r}), \tag{1}$$

where the eigenfunction $\psi_{j\mathbf{k}_\parallel}(\mathbf{r})\equiv\langle\mathbf{r}|j\mathbf{k}_\parallel\rangle$ is defined in Eq. (A16), satisfying $\underline{\mathcal{H}}\psi_{j\mathbf{k}_\parallel}(\mathbf{r})=\mathcal{E}_j(\mathbf{k}_\parallel)\psi_{j\mathbf{k}_\parallel}(\mathbf{r})$, and $\langle j\mathbf{k}_\parallel|j'\mathbf{k}'_\parallel\rangle=\delta_{j,j'}\delta_{\mathbf{k}_\parallel,\mathbf{k}'_\parallel}$. In Eq. (1), $\hat{C}_{j\mathbf{k}_\parallel}(t)$ and $\hat{C}^\dagger_{j\mathbf{k}_\parallel}(t)$ are the annihilation and creation operators for the electron state $|j\mathbf{k}_\parallel\rangle$.

The second-quantization Hamiltonian operator $\hat{\mathcal{H}}_e(t)$ of electrons is defined by [16]

$$\hat{\mathcal{H}}_e(t)=\int d^3\mathbf{r}\hat{\Psi}^\dagger(\mathbf{r},t)\underline{\mathcal{H}}\hat{\Psi}(\mathbf{r},t)=\sum_{j,\mathbf{k}_\parallel}\mathcal{E}_j(\mathbf{k}_\parallel)\hat{C}^\dagger_{j\mathbf{k}_\parallel}(t)\hat{C}_{j\mathbf{k}_\parallel}(t). \tag{2}$$

Using the Fermi-Dirac statistics for the field operators $\hat{\Psi}_j(\mathbf{r},t)$ and $\hat{\Psi}^\dagger_j(\mathbf{r},t)$, we get the following commutator relations:

$$\{\hat{C}_{j\mathbf{k}_\parallel}(t),\hat{C}^\dagger_{j'\mathbf{k}'_\parallel}(t)\}_+=\delta_{j,j'}\delta_{\mathbf{k}_\parallel,\mathbf{k}'_\parallel},$$

$$\{\hat{C}_{j\mathbf{k}_\parallel}(t),\hat{C}_{j'\mathbf{k}'_\parallel}(t)\}_+=\{\hat{C}^\dagger_{j\mathbf{k}_\parallel}(t),\hat{C}^\dagger_{j'\mathbf{k}'_\parallel}(t)\}_+=0, \tag{3}$$

where $\{\hat{\mathcal{F}},\hat{\mathcal{G}}\}_+=\hat{\mathcal{F}}\hat{\mathcal{G}}+\hat{\mathcal{G}}\hat{\mathcal{F}}$ for any operators $\hat{\mathcal{F}}$ and $\hat{\mathcal{G}}$.

Combining electron annihilation and creation operators, we further define the many-particle ascending/descending operators by $\hat{\sigma}_{jj'}(\mathbf{k}_\parallel,t)=\hat{C}^\dagger_{j\mathbf{k}_\parallel}(t)\hat{C}_{j'\mathbf{k}_\parallel}(t)$ for the same wave vector $\mathbf{k}_\parallel$. As a result, the Hamiltonian operator in Eq. (2) can be simply written as

$$\hat{\mathcal{H}}_e(t)=\sum_{j,\mathbf{k}_\parallel}\mathcal{E}_j(\mathbf{k}_\parallel)\hat{\sigma}_{jj}(\mathbf{k}_\parallel,t). \tag{4}$$

B. Quantization of an electromagnetic field

For a spatially uniform electromagnetic field, we can expand its vector potential operator $\hat{\mathbf{A}}(t)$ using the canonical transformation

$$\hat{\mathbf{A}}(t)=\sum_{\mathbf{q},\lambda}\sqrt{\frac{2\pi\hbar c^2\mu_0}{\omega_q\mathcal{V}}}[\hat{a}_{\mathbf{q}\lambda}(t)+\hat{a}^{\dagger}_{\mathbf{q}\lambda}(t)]\mathbf{w}_{\mathbf{q}\lambda}, \tag{5}$$

where $\mathbf{w}_{\mathbf{q}\lambda}$ is the photon unit polarization vector, $\mathbf{q}$ is the photon wave vector, $\lambda=1,2$ is the polarization index with $\mathbf{q}\cdot\mathbf{w}_{\mathbf{q}\lambda}=0$, $\omega_q=qc$ is the photon frequency, $\mathcal{V}$ is the volume of the QW's, and $\hat{a}_{\mathbf{q}\lambda}(t)$ and $\hat{a}^{\dagger}_{\mathbf{q}\lambda}(t)$ are the photon creation and annihilation operators. The uniform-field model is a good approximation to the optical transitions of electrons in QW's as long as $qL_W\ll 1$, where L_W is the well width. By using Eq. (5), the photon Hamiltonian operator takes the form of [1]

$$\hat{\mathcal{H}}_{\rm ph}(t)=\sum_{\mathbf{q},\lambda}\hbar\omega_q\hat{a}^{\dagger}_{\mathbf{q}\lambda}(t)\hat{a}_{\mathbf{q}\lambda}(t). \tag{6}$$

Since photons obey the Bose-Einstein statistics, we get the following commutator relations:

$$\{\hat{a}_{\mathbf{q}\lambda}(t),\hat{a}^{\dagger}_{\mathbf{q}'\lambda'}(t)\}_-=\delta_{\mathbf{q},\mathbf{q}'}\delta_{\lambda,\lambda'},$$

$$\{\hat{a}_{\mathbf{q}\lambda}(t),\hat{a}_{\mathbf{q}'\lambda'}(t)\}_-=\{\hat{a}^{\dagger}_{\mathbf{q}\lambda}(t),\hat{a}^{\dagger}_{\mathbf{q}'\lambda'}(t)\}_-=0, \tag{7}$$

where $\{\hat{\mathcal{F}},\hat{\mathcal{G}}\}_-=\hat{\mathcal{F}}\hat{\mathcal{G}}-\hat{\mathcal{G}}\hat{\mathcal{F}}$ for any operators $\hat{\mathcal{F}}$ and $\hat{\mathcal{G}}$. In the Coulomb gauge, we have $\hat{\mathbf{E}}(t)=-\partial\hat{\mathbf{A}}(t)/\partial t=(i/\hbar)\times[\hat{\mathbf{A}}(t),\hat{\mathcal{H}}_{\rm ph}(t)]_-$. By using Eqs. (5) and (7), the quantized electric field becomes

$$\hat{\mathbf{E}}(t)=i\sum_{\mathbf{q},\lambda}\sqrt{\frac{2\pi\hbar\omega_q}{\epsilon_0\epsilon_r\mathcal{V}}}[\hat{a}_{\mathbf{q}\lambda}(t)-\hat{a}^{\dagger}_{\mathbf{q}\lambda}(t)]\mathbf{w}_{\mathbf{q}\lambda}, \tag{8}$$

where ϵ_r is the average dielectric constant of the QW's. Equations (5), (7), and (8) together lead us to the following relation:

$$\{\hat{\mathbf{A}}(t),\hat{\mathbf{E}}(t)\}_-=-2i\left(\frac{2\pi\hbar}{\epsilon_0\epsilon_r\mathcal{V}}\right)\sum_{\mathbf{q},\lambda}\mathbf{w}_{\mathbf{q}\lambda}\mathbf{w}_{\mathbf{q}\lambda}. \tag{9}$$

C. Quantization of the interaction between electrons and an electromagnetic field

Within the dipole coupling model, the classical form for the interaction between the electrons and an electromagnetic field can be written as

$$\mathcal{H}_{e\text{-ph}}=-e\mathbf{r}(t)\cdot\mathbf{E}(t). \tag{10}$$

By employing the gauge transformation

$$\hat{\mathcal{U}}(t)=\exp\left[\frac{ie}{2\hbar}\mathbf{r}(t)\cdot\hat{\mathbf{A}}(t)\right] \tag{11}$$

and using Eq. (9), the quantized interaction between electrons and photons is [1]

$$\begin{aligned}\hat{\mathcal{H}}_{e\text{-ph}}(t)&=-e\hat{\mathbf{r}}(t)\cdot[\hat{\mathcal{U}}^{\dagger}(t)\hat{\mathbf{E}}(t)\hat{\mathcal{U}}(t)]\\&=-e\hat{\mathbf{r}}(t)\cdot\hat{\mathbf{E}}(t)+\frac{2\pi e^2}{\epsilon_0\epsilon_r\mathcal{V}}\sum_{\mathbf{q},\lambda}[\hat{\mathbf{r}}(t)\cdot\mathbf{w}_{\mathbf{q}\lambda}]^2,\end{aligned} \tag{12}$$

where $\hat{\mathbf{E}}(t)$ is given by Eq. (8) and the last term on the right-hand side of Eq. (12) is the Lamb energy shift. $\hat{\mathbf{r}}(t)$ in Eq. (12) is an operator and is defined as

$$\hat{\mathbf{r}}(t)=\int d^3\mathbf{r}\hat{\Psi}^{\dagger}(\mathbf{r},t)\mathbf{r}\hat{\Psi}(\mathbf{r},t).$$

Combining Eqs. (4), (6), and (12), we get the total Hamiltonian operator for electrons and photons in the QW's,

$$\begin{aligned}\hat{\mathcal{H}}_{\rm tot}(t)=\hat{\mathcal{H}}_e(t)+\hat{\mathcal{H}}_{\rm ph}(t)+\hat{\mathcal{H}}_{e\text{-ph}}(t)&=\sum_{j,\mathbf{k}_\parallel}\mathcal{E}_j(\mathbf{k}_\parallel)\hat{\sigma}_{jj}(\mathbf{k}_\parallel,t)\\&+\sum_{\mathbf{q},\lambda}\hbar\omega_q\hat{a}^{\dagger}_{\mathbf{q}\lambda}(t)\hat{a}_{\mathbf{q}\lambda}(t)\\&+i\hbar\sum_{jj',\mathbf{k}_\parallel}\mathcal{I}_{\mathbf{q}\lambda,jj'}(\mathbf{k}_\parallel)\hat{\sigma}_{jj'}(\mathbf{k}_\parallel,t)[\hat{a}_{\mathbf{q}\lambda}(t)-\hat{a}^{\dagger}_{\mathbf{q}\lambda}(t)]\\&+\frac{2e^2}{3\pi\epsilon_0\epsilon_r c^3}\int_0^{+\infty}d\omega_q\omega_q^2\sum_{jj',\mathbf{k}_\parallel}r^2_{jj'}(\mathbf{k}_\parallel)\hat{\sigma}_{jj'}(\mathbf{k}_\parallel,t),\end{aligned} \tag{13}$$

where the last term is the Lamb energy shift related to the electron self-energy, which will be neglected as a standard approximation [1] in the following. The electron-photon coupling matrix in Eq. (13) is

$$\mathcal{I}_{\mathbf{q}\lambda,jj'}(\mathbf{k}_\parallel)=-\frac{e}{\hbar}\sqrt{\frac{2\pi\hbar\omega_q}{\epsilon_0\epsilon_r\mathcal{V}}}\mathbf{w}_{\mathbf{q}\lambda}\cdot\mathbf{r}_{jj'}(\mathbf{k}_\parallel), \tag{14}$$

with $\mathbf{r}_{jj'}(\mathbf{k}_\parallel)=\langle j\mathbf{k}_\parallel|\mathbf{r}|j'\mathbf{k}_\parallel\rangle$.

III. EQUATIONS OF MOTION

By working within the Heisenberg picture, the equations of motion for photons take the form of

$$\frac{d}{dt}\begin{bmatrix}\hat{a}_{\mathbf{q}\lambda}(t)\\ \hat{a}^{\dagger}_{\mathbf{q}\lambda}(t)\end{bmatrix}=\frac{1}{i\hbar}\left\{\begin{bmatrix}\hat{a}_{\mathbf{q}\lambda}(t)\\ \hat{a}^{\dagger}_{\mathbf{q}\lambda}(t)\end{bmatrix},\hat{\mathcal{H}}_{\rm tot}(t)\right\}_-, \tag{15}$$

which have the following solution:

$$\begin{aligned}\begin{bmatrix}\hat{a}_{\mathbf{q}\lambda}(t)\\ \hat{a}^{\dagger}_{\mathbf{q}\lambda}(t)\end{bmatrix}&=\begin{bmatrix}\hat{a}_{\mathbf{q}\lambda}(0)e^{-i\omega_q t}\\ \hat{a}^{\dagger}_{\mathbf{q}\lambda}(0)e^{i\omega_q t}\end{bmatrix}-\sum_{jj',\mathbf{k}_\parallel}\mathcal{I}_{\mathbf{q}\lambda,jj'}(\mathbf{k}_\parallel)\\&\times\int_0^t dt'\hat{\sigma}_{jj'}(\mathbf{k}_\parallel,t')\begin{bmatrix}e^{i\omega_q(t'-t)}\\ e^{-i\omega_q(t'-t)}\end{bmatrix}.\end{aligned} \tag{16}$$

The second term in Eq. (16) represents the contribution from the coupling between the electrons and photons. Under the vacuum-field approximation, we can set $\hat{a}_{\mathbf{q}\lambda}(0)=\hat{a}^{\dagger}_{\mathbf{q}\lambda}(0)=0$.

For electrons, the commutator relations in Eq. (3) lead to

$$\{\hat{\sigma}_{ii'}(\mathbf{k}_{\parallel},t),\hat{\sigma}_{jj'}(\mathbf{k}'_{\parallel},t)\}_{-}=\delta_{\mathbf{k}_{\parallel},\mathbf{k}'_{\parallel}}[\delta_{i'j}\hat{\sigma}_{ij'}(\mathbf{k}_{\parallel},t)-\delta_{j'i}\hat{\sigma}_{ji'}(\mathbf{k}_{\parallel},t)]. \tag{17}$$

As a result, the equations of motion for electrons in the Heisenberg picture are

$$\begin{aligned}\frac{d}{dt}\hat{\sigma}_{lm}(\mathbf{p}_{\parallel},t)&=\frac{1}{i\hbar}\{\hat{\sigma}_{lm}(\mathbf{p}_{\parallel},t),\hat{\mathcal{H}}_{\mathrm{tot}}(t)\}_{-}\\&=-i\Omega_{ml}(\mathbf{p}_{\parallel})\hat{\sigma}_{lm}(\mathbf{p}_{\parallel},t)\\&\quad+\sum_{\mathbf{q},\lambda}\sum_{jj'}[\delta_{mj}\hat{\sigma}_{lj'}(\mathbf{p}_{\parallel},t)\\&\quad-\delta_{j'l}\hat{\sigma}_{jm}(\mathbf{p}_{\parallel},t)]\mathcal{I}_{\mathbf{q}\lambda,jj'}(\mathbf{p}_{\parallel})\hat{a}_{\mathbf{q}\lambda}(t)\\&\quad-\sum_{\mathbf{q},\lambda}\sum_{jj'}\hat{a}^{\dagger}_{\mathbf{q}\lambda}(t)[\delta_{mj}\hat{\sigma}_{lj'}(\mathbf{p}_{\parallel},t)\\&\quad-\delta_{j'l}\hat{\sigma}_{jm}(\mathbf{p}_{\parallel},t)]\mathcal{I}_{\mathbf{q}\lambda,jj'}(\mathbf{p}_{\parallel}),\end{aligned} \tag{18}$$

where $\Omega_{ml}(\mathbf{p}_{\parallel})=[\mathcal{E}_m(\mathbf{p}_{\parallel})-\mathcal{E}_l(\mathbf{p}_{\parallel})]/\hbar$. Because a uniform electromagnetic field is assumed, the electron transitions in Eq. (18) consist of vertical ones. Substituting Eq. (16) into Eq. (18) under the vacuum-field approximation, we get

$$\begin{aligned}\frac{d}{dt}\hat{\sigma}_{lm}(\mathbf{p}_{\parallel},t)&=-i\Omega_{ml}(\mathbf{p}_{\parallel})\hat{\sigma}_{lm}(\mathbf{p}_{\parallel},t)-\sum_{\mathbf{q},\lambda}\sum_{jj'}[\delta_{mj}\hat{\sigma}_{lj'}(\mathbf{p}_{\parallel},t)\\&\quad-\delta_{j'l}\hat{\sigma}_{jm}(\mathbf{p}_{\parallel},t)]\mathcal{I}_{\mathbf{q}\lambda,jj'}(\mathbf{p}_{\parallel})\\&\quad\times\left\{\sum_{ii',\mathbf{k}_{\parallel}}\mathcal{I}_{\mathbf{q}\lambda,ii'}(\mathbf{k}_{\parallel})\int_0^t dt'\,\hat{\sigma}_{ii'}(\mathbf{k}_{\parallel},t')\right.\\&\quad\left.\times e^{i\omega_q(t'-t)}\right\}+\sum_{\mathbf{q},\lambda}\sum_{jj'}\left\{\sum_{ii',\mathbf{k}_{\parallel}}\mathcal{I}_{\mathbf{q}\lambda,ii'}(\mathbf{k}_{\parallel})\right.\\&\quad\left.\times\int_0^t dt'\,\hat{\sigma}_{ii'}(\mathbf{k}_{\parallel},t')e^{-i\omega_q(t'-t)}\right\}\\&\quad\times[\delta_{mj}\hat{\sigma}_{lj'}(\mathbf{p}_{\parallel},t)-\delta_{j'l}\hat{\sigma}_{jm}(\mathbf{p}_{\parallel},t)]\mathcal{I}_{\mathbf{q}\lambda,jj'}(\mathbf{p}_{\parallel}),\end{aligned} \tag{19}$$

where the last two terms correspond to the coupling between electrons and spontaneous photons emitted by the radiative decay of excited electrons in the QW's.

A. Adiabatic approximation

If we assume a weak interaction between the electrons and spontaneous photons (not pump-laser photons as introduced below), the perturbed electron states should evolve very similarly to the free-electron evolution in a first-order approximation [1]. This implies that

$$\hat{\sigma}_{ii'}(\mathbf{k}_{\parallel},t')\approx\hat{\sigma}_{jj'}(\mathbf{k}_{\parallel},t)e^{-i\Omega_{i'i}(\mathbf{k}_{\parallel})(t'-t)}. \tag{20}$$

The free-electron evolution employed in Eq. (20) is usually termed the *adiabatic approximation*.

B. Long-time limit

If we further assume $\omega_q\neq\Omega_{jj'}(\mathbf{k}_{\parallel})$ and $t\gg 1/\Omega_{jj'}(\mathbf{k}_{\parallel})$ (such as in a steady state) for any j, j', and $\mathbf{k}_{\parallel}$, the time integral in Eq. (19) can be evaluated analytically and becomes independent of time t. In this *long-time limit*, we find [1]

$$\begin{aligned}&\int_0^t dt'\exp\{i[\omega_q-\Omega_{jj'}(\mathbf{k}_{\parallel})](t'-t)\}\\&\quad\approx\pi\delta[\omega_q-\Omega_{jj'}(\mathbf{k}_{\parallel})]-i\mathcal{P}\left[\frac{1}{\omega_q-\Omega_{jj'}(\mathbf{k}_{\parallel})}\right],\end{aligned} \tag{21}$$

where $\mathcal{P}[\cdots]$ stands for taking only the principal value of $[\cdots]$.

C. First simplification of the equations of motion

By using the *adiabatic approximation* in Eq. (20) and the *long-time limit* in Eq. (21), the previous equations of motion in Eq. (19) are simplified as

$$\begin{aligned}\frac{d}{dt}\hat{\sigma}_{lm}(\mathbf{p}_{\parallel},t)&=-i\Omega_{ml}(\mathbf{p}_{\parallel})\hat{\sigma}_{lm}(\mathbf{p}_{\parallel},t)\\&\quad-\sum_{j'}\{\beta_{mj',j'm}[\mathbf{p}_{\parallel},\Omega_{mj'}(\mathbf{p}_{\parallel})]\\&\quad+\beta_{lj',j'l}[\mathbf{p}_{\parallel},\Omega_{lj'}(\mathbf{p}_{\parallel})]\}\hat{\sigma}_{lm}(\mathbf{p}_{\parallel},t)\\&\quad-\sum_{j'}\sum_{i'\neq m}\Gamma_{mj',j'i'}[\mathbf{p}_{\parallel},\Omega_{i'j'}(\mathbf{p}_{\parallel})]\hat{\sigma}_{li'}(\mathbf{p}_{\parallel},t)\\&\quad-\sum_{j'}\sum_{i'\neq l}\Gamma^{*}_{lj',j'i'}[\mathbf{p}_{\parallel},\Omega_{i'j'}(\mathbf{p}_{\parallel})]\hat{\sigma}_{i'm}(\mathbf{p}_{\parallel},t)\\&\quad+\sum_{j'i'}\Gamma_{j'l,mi'}[\mathbf{p}_{\parallel},\Omega_{i'm}(\mathbf{p}_{\parallel})]\hat{\sigma}_{j'i'}(\mathbf{p}_{\parallel},t)\\&\quad+\sum_{j'i'}\Gamma^{*}_{j'm,li'}[\mathbf{p}_{\parallel},\Omega_{i'l}(\mathbf{p}_{\parallel})]\hat{\sigma}_{i'j'}(\mathbf{p}_{\parallel},t),\end{aligned} \tag{22}$$

where the radiative-decay coupling matrix

$$\Gamma_{jj',ii'}[\mathbf{k}_{\parallel},\Omega_{i'i}(\mathbf{k}_{\parallel})]=\beta_{jj',ii'}[\mathbf{k}_{\parallel},\Omega_{i'i}(\mathbf{k}_{\parallel})]-i\gamma_{jj',ii'}[\mathbf{k}_{\parallel},\Omega_{i'i}(\mathbf{k}_{\parallel})]$$

with

$$\beta_{jj',ii'}[\mathbf{k}_\parallel,\Omega_{i'i}(\mathbf{k}_\parallel)]=\frac{2e^2\Omega_{i'i}^3(\mathbf{k}_\parallel)}{3\hbar\epsilon_0\epsilon_r c^3}\theta[\Omega_{i'i}(\mathbf{k}_\parallel)]\times[\mathbf{r}_{jj'}(\mathbf{k}_\parallel)\cdot\mathbf{r}_{ii'}(\mathbf{k}_\parallel)], \quad (23)$$

$$\gamma_{jj',ii'}[\mathbf{k}_\parallel,\Omega_{i'i}(\mathbf{k}_\parallel)]=\frac{2e^2}{3\pi\hbar\epsilon_0\epsilon_r c^3}\times[\mathbf{r}_{jj'}(\mathbf{k}_\parallel)\cdot\mathbf{r}_{ii'}(\mathbf{k}_\parallel)]\times\mathcal{P}\left[\int_0^{+\infty}\frac{\omega_q^3 d\omega_q}{\omega_q-\Omega_{i'i}(\mathbf{k}_\parallel)}\right]. \quad (24)$$

Here, $\theta(x)$ in Eq. (23) is the Heaviside step function. $\gamma_{jj',ii'}[\mathbf{k}_\parallel,\Omega_{i'i}(\mathbf{k}_\parallel)]$ is on the same order of magnitude as the electron self-energy and will be neglected thereafter as a standard approximation [1].

D. Second simplification of the equations of motion

By keeping only the real part of $\Gamma_{jj',ii'}[\mathbf{k}_\parallel,\Omega_{i'i}(\mathbf{k}_\parallel)]$ in Eq. (22), we are finally led to the simplified equations of motion,

$$\begin{aligned}\frac{d}{dt}\hat{\sigma}_{lm}(\mathbf{p}_\parallel,t)=&-i\Omega_{ml}(\mathbf{p}_\parallel)\hat{\sigma}_{lm}(\mathbf{p}_\parallel,t)\\&-\left[\frac{1}{\tau_l(\mathbf{p}_\parallel)}+\frac{1}{\tau_m(\mathbf{p}_\parallel)}\right]\hat{\sigma}_{lm}(\mathbf{p}_\parallel,t)\\&-\sum_{j'}\left\{\sum_{i'\neq m}\beta_{mj',j'i'}[\mathbf{p}_\parallel,\Omega_{i'j'}(\mathbf{p}_\parallel)]\hat{\sigma}_{li'}(\mathbf{p}_\parallel,t)\right.\\&\left.+\sum_{i'\neq l}\beta_{lj',j'i'}[\mathbf{p}_\parallel,\Omega_{i'j'}(\mathbf{p}_\parallel)]\hat{\sigma}_{i'm}(\mathbf{p}_\parallel,t)\right\}\\&+\sum_{j'i'}\{\beta_{j'l,mi'}[\mathbf{p}_\parallel,\Omega_{i'm}(\mathbf{p}_\parallel)]\\&+\beta_{i'm,lj'}[\mathbf{p}_\parallel,\Omega_{i'l}(\mathbf{p}_\parallel)]\}\hat{\sigma}_{j'i'}(\mathbf{p}_\parallel,t), \quad (25)\end{aligned}$$

where the radiative-decay rate is

$$\frac{1}{\tau_j(\mathbf{k}_\parallel)}=\sum_{i<j}\beta_{ji,ij}[\mathbf{k}_\parallel,\Omega_{ji}(\mathbf{k}_\parallel)]. \quad (26)$$

The last two terms on the right-hand side of Eq. (25) contain ODRDC between a pair of electron transitions. This leads to quantum interference when these two electron transitions become nearly degenerate.

IV. DENSITY-MATRIX EQUATIONS UNDER AN EXTERNAL LASER FIELD

From quantum statistics, we know that for any physical operator $\hat{\mathcal{B}}(\mathbf{r},t)$, only its quantum-statistical average is an observable quantity and can be computed by taking the trace of the product of it with the system density operator $\hat{\rho}(\mathbf{r},t)$ [16]. The density-matrix $\rho_{ml}(\mathbf{k}_\parallel,t)$ of the system is given by the quantum-statistical average of the many-particle ascending/descending operators $\hat{\sigma}_{lm}(\mathbf{k}_\parallel,t)$.

In this paper, the spontaneous electromagnetic field from the radiative decay of electrons is treated within the quantum electrodynamic limit, but the external laser field will only be treated classically [2]. This introduces an additional dipole-coupling term $-e\hat{\mathbf{r}}(t)\cdot\mathbf{E}_L(t)$ to the total Hamiltonian operator in Eq. (13), where $\mathbf{E}_L(t)$ is a spatially uniform laser field. Including the interaction of electrons with $\mathbf{E}_L(t)$, we arrive at the following density-matrix equations from Eq. (25):

$$\begin{aligned}\frac{d}{dt}\rho_{ml}(\mathbf{p}_\parallel,t)=&-i\Omega_{ml}(\mathbf{p}_\parallel)\rho_{ml}(\mathbf{p}_\parallel,t)\\&-\left[\frac{1}{\tau_l(\mathbf{p}_\parallel)}+\frac{1}{\tau_m(\mathbf{p}_\parallel)}\right]\rho_{ml}(\mathbf{p}_\parallel,t)\\&+\frac{ie}{\hbar}\mathbf{E}_L(t)\cdot\sum_j[\mathbf{r}_{mj}(\mathbf{p}_\parallel)\rho_{jl}(\mathbf{p}_\parallel,t)\\&-\mathbf{r}_{jl}(\mathbf{p}_\parallel)\rho_{mj}(\mathbf{p}_\parallel,t)]\\&-\sum_{j'}\left\{\sum_{i'\neq m}\beta_{mj',j'i'}[\mathbf{p}_\parallel,\Omega_{i'j'}(\mathbf{p}_\parallel)]\rho_{i'l}(\mathbf{p}_\parallel,t)\right.\\&\left.+\sum_{i'\neq l}\beta_{lj',j'i'}[\mathbf{p}_\parallel,\Omega_{i'j'}(\mathbf{p}_\parallel)]\rho_{mi'}(\mathbf{p}_\parallel,t)\right\}\\&+\sum_{j'i'}\{\beta_{j'l,mi'}[\mathbf{p}_\parallel,\Omega_{i'm}(\mathbf{p}_\parallel)]\\&+\beta_{i'm,lj'}[\mathbf{p}_\parallel,\Omega_{i'l}(\mathbf{p}_\parallel)]\}\rho_{i'j'}(\mathbf{p}_\parallel,t). \quad (27)\end{aligned}$$

In the following, we will explicitly write out the equations of motion in Eq. (27) for the two- or three-level models.

A. Two-level model

For a system that has only two relevant electronic states whose energy separation closes to the pump-laser photon energy $\hbar\omega_L$, we get from Eq. (27)

$$\frac{d}{dt}\rho_{11}(\mathbf{k}_\parallel,t)=\frac{2}{\tau_2(\mathbf{k}_\parallel)}\rho_{22}(\mathbf{k}_\parallel,t)-\frac{2e}{\hbar}\mathbf{E}_L(t)\cdot\mathbf{r}_{12}(\mathbf{k}_\parallel)\mathrm{Im}[\rho_{12}^*(\mathbf{k}_\parallel,t)], \quad (28)$$

$$\begin{aligned}\frac{d}{dt}\rho_{12}(\mathbf{k}_\parallel,t)=&\,i\Omega_{21}(\mathbf{k}_\parallel)\rho_{12}(\mathbf{k}_\parallel,t)\\&-\frac{1}{\tau_2(\mathbf{k}_\parallel)}\rho_{12}(\mathbf{k}_\parallel,t)+\frac{ie}{\hbar}\mathbf{E}_L(t)\cdot\mathbf{r}_{12}(\mathbf{k}_\parallel)\\&\times[\rho_{22}(\mathbf{k}_\parallel,t)-\rho_{11}(\mathbf{k}_\parallel,t)]\\&+\beta_{12,12}[\mathbf{k}_\parallel,\Omega_{21}(\mathbf{k}_\parallel)]\rho_{12}^*(\mathbf{k}_\parallel,t). \quad (29)\end{aligned}$$

Moreover, we have $d/dt\,[\rho_{11}(\mathbf{k}_\parallel,t)+\rho_{22}(\mathbf{k}_\parallel,t)]=0$ for a closed system that has no exchange of electrons with the outside. There is only one ODRDC-related term containing $\beta_{12,12}[\mathbf{k}_\parallel,\Omega_{21}(\mathbf{k}_\parallel)]$ in Eq. (29), and it can be neglected under the rotating-wave approximation described below. In this regard, the two-level system is trivial with no ODRDC because it lacks two nearly degenerate electron transitions in the system.

B. Three-level model

For a system that has three relevant electronic states, we find from Eq. (27)

$$\frac{d}{dt}\rho_{11}(\mathbf{k}_\parallel,t)=2\beta_{21,12}[\mathbf{k}_\parallel,\Omega_{21}(\mathbf{k}_\parallel)]\rho_{22}(\mathbf{k}_\parallel,t)+2\beta_{31,13}[\mathbf{k}_\parallel,\Omega_{31}(\mathbf{k}_\parallel)]\rho_{33}(\mathbf{k}_\parallel,t)$$
$$-\frac{2e}{\hbar}\mathbf{E}_L(t)\cdot\mathbf{r}_{12}(\mathbf{k}_\parallel)\mathrm{Im}[\rho_{12}^*(\mathbf{k}_\parallel,t)]-\frac{2e}{\hbar}\mathbf{E}_L(t)\cdot\mathbf{r}_{13}(\mathbf{k}_\parallel)\mathrm{Im}[\rho_{13}^*(\mathbf{k}_\parallel,t)]$$
$$-2\beta_{12,23}[\mathbf{k}_\parallel,\Omega_{32}(\mathbf{k}_\parallel)]\mathrm{Re}[\rho_{13}(\mathbf{k}_\parallel,t)]+2\{\beta_{31,12}[\mathbf{k}_\parallel,\Omega_{21}(\mathbf{k}_\parallel)]+\beta_{21,13}[\mathbf{k}_\parallel,\Omega_{31}(\mathbf{k}_\parallel)]\}\mathrm{Re}[\rho_{23}(\mathbf{k}_\parallel,t)], \quad (30)$$

$$\frac{d}{dt}\rho_{22}(\mathbf{k}_\parallel,t)=-\frac{2}{\tau_2(\mathbf{k}_\parallel)}\rho_{22}(\mathbf{k}_\parallel,t)+2\beta_{32,23}[\mathbf{k}_\parallel,\Omega_{32}(\mathbf{k}_\parallel)]\rho_{33}(\mathbf{k}_\parallel,t)$$
$$-\frac{2e}{\hbar}\mathbf{E}_L(t)\cdot\mathbf{r}_{23}(\mathbf{k}_\parallel)\mathrm{Im}[\rho_{23}^*(\mathbf{k}_\parallel,t)]-\frac{2e}{\hbar}\mathbf{E}_L(t)\cdot\mathbf{r}_{12}(\mathbf{k}_\parallel)\mathrm{Im}[\rho_{12}(\mathbf{k}_\parallel,t)]$$
$$+2\beta_{12,23}[\mathbf{k}_\parallel,\Omega_{32}(\mathbf{k}_\parallel)]\mathrm{Re}[\rho_{13}(\mathbf{k}_\parallel,t)]-2\beta_{21,13}[\mathbf{k}_\parallel,\Omega_{31}(\mathbf{k}_\parallel)]\mathrm{Re}[\rho_{23}(\mathbf{k}_\parallel,t)], \quad (31)$$

$$\frac{d}{dt}\rho_{12}(\mathbf{k}_\parallel,t)=i\Omega_{21}(\mathbf{k}_\parallel)\rho_{12}(\mathbf{k}_\parallel,t)-\frac{1}{\tau_2(\mathbf{k}_\parallel)}\rho_{12}(\mathbf{k}_\parallel,t)+\{\beta_{32,13}[\mathbf{k}_\parallel,\Omega_{31}(\mathbf{k}_\parallel)]+\beta_{31,23}[\mathbf{k}_\parallel,\Omega_{32}(\mathbf{k}_\parallel)]\}\rho_{33}(\mathbf{k}_\parallel,t)$$
$$+\frac{ie}{\hbar}\mathbf{E}_L(t)\cdot\mathbf{r}_{12}(\mathbf{k}_\parallel)[\rho_{22}(\mathbf{k}_\parallel,t)-\rho_{11}(\mathbf{k}_\parallel,t)]+\frac{ie}{\hbar}\mathbf{E}_L(t)\cdot\mathbf{r}_{13}(\mathbf{k}_\parallel)\rho_{23}^*(\mathbf{k}_\parallel,t)-\frac{ie}{\hbar}\mathbf{E}_L(t)\cdot\mathbf{r}_{23}^*(\mathbf{k}_\parallel)\rho_{13}(\mathbf{k}_\parallel,t)$$
$$+\beta_{12,12}[\mathbf{k}_\parallel,\Omega_{21}(\mathbf{k}_\parallel)]\rho_{12}^*(\mathbf{k}_\parallel,t)+\beta_{12,13}[\mathbf{k}_\parallel,\Omega_{31}(\mathbf{k}_\parallel)]\rho_{13}^*(\mathbf{k}_\parallel,t)+\{\beta_{21,23}[\mathbf{k}_\parallel,\Omega_{32}(\mathbf{k}_\parallel)]$$
$$+\beta_{32,12}[\mathbf{k}_\parallel,\Omega_{21}(\mathbf{k}_\parallel)]\}\rho_{23}(\mathbf{k}_\parallel,t)-\{\beta_{12,23}[\mathbf{k}_\parallel,\Omega_{32}(\mathbf{k}_\parallel)]\rho_{23}^*(\mathbf{k}_\parallel,t)+\beta_{21,13}[\mathbf{k}_\parallel,\Omega_{31}(\mathbf{k}_\parallel)]\rho_{13}(\mathbf{k}_\parallel,t)\}, \quad (32)$$

$$\frac{d}{dt}\rho_{13}(\mathbf{k}_\parallel,t)=i\Omega_{31}(\mathbf{k}_\parallel)\rho_{13}(\mathbf{k}_\parallel,t)-\frac{1}{\tau_3(\mathbf{k}_\parallel)}\rho_{13}(\mathbf{k}_\parallel,t)+\beta_{23,12}[\mathbf{k}_\parallel,\Omega_{21}(\mathbf{k}_\parallel)]\rho_{22}(\mathbf{k}_\parallel,t)+\frac{ie}{\hbar}\mathbf{E}_L(t)\cdot\mathbf{r}_{13}(\mathbf{k}_\parallel)[\rho_{33}(\mathbf{k}_\parallel,t)$$
$$-\rho_{11}(\mathbf{k}_\parallel,t)]+\frac{ie}{\hbar}\mathbf{E}_L(t)\cdot\mathbf{r}_{12}(\mathbf{k}_\parallel)\rho_{23}(\mathbf{k}_\parallel,t)-\frac{ie}{\hbar}\mathbf{E}_L(t)\cdot\mathbf{r}_{23}(\mathbf{k}_\parallel)\rho_{12}(\mathbf{k}_\parallel,t)+\beta_{13,13}[\mathbf{k}_\parallel,\Omega_{31}(\mathbf{k}_\parallel)]\rho_{13}^*(\mathbf{k}_\parallel,t)$$
$$+\beta_{13,12}[\mathbf{k}_\parallel,\Omega_{21}(\mathbf{k}_\parallel)]\rho_{12}^*(\mathbf{k}_\parallel,t)+\beta_{23,13}[\mathbf{k}_\parallel,\Omega_{31}(\mathbf{k}_\parallel)]\rho_{23}^*(\mathbf{k}_\parallel,t)-\{\beta_{12,23}[\mathbf{k}_\parallel,\Omega_{32}(\mathbf{k}_\parallel)]\rho_{33}(\mathbf{k}_\parallel,t)$$
$$+\beta_{31,12}[\mathbf{k}_\parallel,\Omega_{31}(\mathbf{k}_\parallel)]\rho_{12}(\mathbf{k}_\parallel,t)\}, \quad (33)$$

$$\frac{d}{dt}\rho_{23}(\mathbf{k}_\parallel,t)=i\Omega_{32}(\mathbf{k}_\parallel)\rho_{23}(\mathbf{k}_\parallel,t)-\left[\frac{1}{\tau_2(\mathbf{k}_\parallel)}+\frac{1}{\tau_3(\mathbf{k}_\parallel)}\right]\rho_{23}(\mathbf{k}_\parallel,t)+\frac{ie}{\hbar}\mathbf{E}_L(t)\cdot\mathbf{r}_{23}(\mathbf{k}_\parallel)[\rho_{33}(\mathbf{k}_\parallel,t)-\rho_{22}(\mathbf{k}_\parallel,t)]$$
$$+\frac{ie}{\hbar}\mathbf{E}_L(t)\cdot\mathbf{r}_{12}^*(\mathbf{k}_\parallel)\rho_{13}(\mathbf{k}_\parallel,t)-\frac{ie}{\hbar}\mathbf{E}_L(t)\cdot\mathbf{r}_{13}(\mathbf{k}_\parallel)\rho_{12}^*(\mathbf{k}_\parallel,t)+\beta_{23,23}[\mathbf{k}_\parallel,\Omega_{32}(\mathbf{k}_\parallel)]\rho_{23}^*(\mathbf{k}_\parallel,t)$$
$$+\beta_{13,23}[\mathbf{k}_\parallel,\Omega_{32}(\mathbf{k}_\parallel)]\rho_{13}^*(\mathbf{k}_\parallel,t)-\{\beta_{21,13}[\mathbf{k}_\parallel,\Omega_{31}(\mathbf{k}_\parallel)]\rho_{33}(\mathbf{k}_\parallel,t)+\beta_{31,12}[\mathbf{k}_\parallel,\Omega_{21}(\mathbf{k}_\parallel)]\rho_{22}(\mathbf{k}_\parallel,t)\}. \quad (34)$$

Furthermore, we get $d/dt[\rho_{11}(\mathbf{k}_\parallel,t)+\rho_{22}(\mathbf{k}_\parallel,t)+\rho_{33}(\mathbf{k}_\parallel,t)]=0$ for a closed system with a fixed number of electrons.

V. RESONANT DOUBLE QUANTUM WELLS PUMPED BY A LASER

In this section, the density-matrix equations are first simplified under the *rotating-wave approximation* [2], where only the nearly resonant terms in the density-matrix equations are kept, for three-level unstrained RADQW's with laser pumping. After this, the formulas for time-resolved absorption and photoluminescence are derived for electrons in the RADQW's.

A. Laser-coupled three-level asymmetric double quantum wells

When $\mathbf{k}_\parallel=0$, the heavy- and light-hole states decouple from each other (the off-diagonal matrix elements in the Lüttinger four-band $\mathbf{k}\cdot\mathbf{p}$ Hamiltonian become zero). The couplings between the conduction and valence bands or between the spin-orbit split and hole valence bands are all very small due to the large energy separation between these bands. As a result, $\mathcal{H}^{\mathbf{k}\cdot\mathbf{p}}+\mathcal{H}^{\mathrm{SO}}$ in Eq. (A1) becomes nearly diagonal. Although the existence of strain terms $\mathcal{D}^{\mathbf{k}\cdot\mathbf{p}}+\mathcal{D}^{\mathrm{SO}}$ in Eq. (A1) can still couple different bands, they are absent for the unstrained QW's. From now on, we consider only the unstrained QW's. In order to discuss the hole states clearly, we define the light- and heavy-hole states as follows. The heavy-hole states refer to the filled valence-band states $[u_4^B(\mathbf{r}),u_5^B(\mathbf{r})]$ [see Eq. (A20)] with a heavier effective mass in the z direction but a lighter effective mass within the QW plane. The light-hole states refer to the filled valence-band states $[u_3^B(\mathbf{r}),u_6^B(\mathbf{r})]$ with a lighter effective mass in the z direction but a heavier effective mass within the QW plane. We know that even though the heavy- and light-hole states become degenerate at $\mathbf{k}=0$ in zinc-blende bulk materials, they are still separated at $\mathbf{k}_\parallel=0$ in the QW's due to the different effective masses of heavy and light holes in the z direction.

For interband pumping, we consider an undoped RADQW as shown in Fig. 1(a). For the conduction band, the only confined electron state E_1^L in the deep and narrow left QW is aligned with the ground state E_1^R of electrons in the shallow and wide right QW, forming a tunneling-split doublet. For the valence band, the topmost hole state H_1^L is a heavy-hole state confined in the left QW. We will denote it by $|1\mathbf{k}_\parallel\rangle$ and the electron doublet in both QW's by $|2\mathbf{k}_\parallel\rangle$ and $|3\mathbf{k}_\parallel\rangle$. We further assume that an external laser field $\mathbf{E}_L(t)$ polarized in the QW plane is applied to the RADQW's. This laser field will excite electrons from the lower hole state to the upper electron doublet, shown by two thick dashed arrows in (a). The laser photon energy $\hbar\omega_L$ is set close to the energy separation between the ground heavy-hole state and the electron doublet. As a result, we can consider only three relevant states

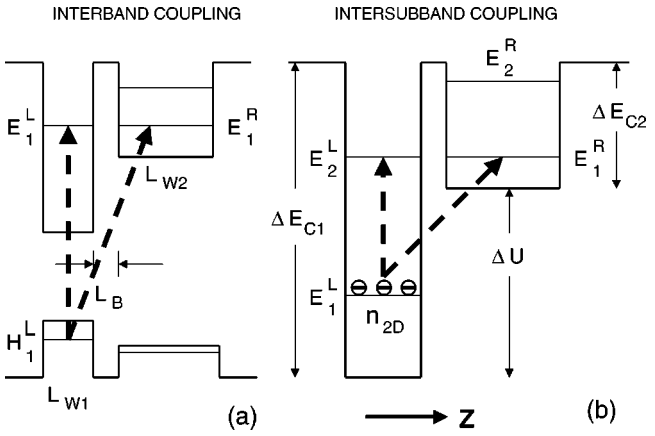

FIG. 1. Illustration of RADQW's with interband [in (a)] and intersubband [in (b)] pumping. The barrier material of RADQW's is $Al_{0.35}Ga_{0.65}As$, and the materials for the left and right QW's are GaAs and $Al_{0.208}Ga_{0.792}As$, respectively. Two nearly degenerate electron transitions in the system are indicated by the thick dashed arrows. L_{W1} and L_{W2} are the widths of the left and right QW's, and L_B is the thickness of the middle barrier. ΔE_{C1} and ΔE_{C2} are the conduction-band offsets for the left and right QW's, and ΔU is the step height between the bottoms of the two QW's in the conduction band. In (a), $\mathbf{E}_L(t)$ and $\mathbf{E}_P(t)$ are chosen to be polarized within the QW plane. In (b), $\mathbf{E}_L(t)$ and $\mathbf{E}_P(t)$ are assumed to be polarized in the z direction. The sample used in our numerical calculation is shown in (b) with doped electron density n_{2D} indicated by three circles filled with ''$-$'' signs at their centers. All the parameters for this sample are summarized in Tables I and II.

$|j\mathbf{k}_\parallel\rangle$ with $j=1,2,3$ for this interband laser-coupled RADQW, where the hole envelope function is strongly $k_\parallel$-dependent.

For intersubband pumping, on the other hand, we consider a doped RADQW as shown in Fig. 1(b), where the electrons released from ionized donors in the left QW are illustrated by three circles filled with ''$-$'' signs at their centers. In this case, the hole states are irrelevant and the electron envelope function is approximately $k_\parallel$-independent. For the conduction band, the left deep and narrow QW contains two confined electron states E_1^L and E_2^L. The upper level E_2^L in the left QW is aligned with the ground level E_1^R of electrons in the right QW, producing a tunneling-split doublet. We will denote E_1^L in the conduction band by $|1\mathbf{k}_\parallel\rangle$, and the doublet by $|2\mathbf{k}_\parallel\rangle$ and $|3\mathbf{k}_\parallel\rangle$. For this doped RADQW, we assume that $\mathbf{E}_L(t)$ is polarized in the z direction and $\hbar\omega_L$ is set close to the energy difference between the ground state and the doublet. Consequently, we will consider only three electronic states $|j\mathbf{k}_\parallel\rangle$ with $j=1,2,3$ for this intersubband laser-coupled RADQW.

We will now obtain the density-matrix equations relevant to interband or intersubband pumping in a three-level RADQW with laser pumping. By using the rotating-wave approximation under the condition $\hbar\omega_L\approx\Omega_{21}(k_\parallel),\Omega_{31}(k_\parallel)$ and $\hbar\omega_L\gg\Omega_{32}(k_\parallel)$, we can simplify the density-matrix equations in Eqs. (30)–(34) by keeping only the nearly resonant terms,

$$\frac{d}{dt}\rho_{11}(k_\parallel,t)=2\beta_{21,12}[\Omega_{21}(k_\parallel)]\rho_{22}(k_\parallel,t)+2\beta_{31,13}[\Omega_{31}(k_\parallel)]\rho_{33}(k_\parallel,t)$$
$$+\frac{2e}{\hbar}\mathbf{E}_L(t)\cdot\mathbf{r}_{12}(\mathbf{k}_\parallel)\mathrm{Im}[\rho_{12}(k_\parallel,t)]+\frac{2e}{\hbar}\mathbf{E}_L(t)\cdot\mathbf{r}_{13}(\mathbf{k}_\parallel)\mathrm{Im}[\rho_{13}(k_\parallel,t)]$$
$$+2\{\beta_{31,12}[\Omega_{21}(k_\parallel)]+\beta_{21,13}[\Omega_{31}(k_\parallel)]\}\mathrm{Re}[\rho_{23}(k_\parallel,t)], \tag{35}$$

$$\frac{d}{dt}\rho_{22}(k_\parallel,t)=-\frac{2}{\tau_2(k_\parallel)}\rho_{22}(k_\parallel,t)+2\beta_{32,23}[\Omega_{32}(k_\parallel)]\rho_{33}(k_\parallel,t)$$
$$-\frac{2e}{\hbar}\mathbf{E}_L(t)\cdot\mathbf{r}_{12}(\mathbf{k}_\parallel)\mathrm{Im}[\rho_{12}(k_\parallel,t)]-2\beta_{21,13}[\Omega_{31}(k_\parallel)]\mathrm{Re}[\rho_{23}(k_\parallel,t)], \tag{36}$$

$$\frac{d}{dt}\rho_{12}(k_\parallel,t)=i\Omega_{21}(k_\parallel)\rho_{12}(k_\parallel,t)-\frac{1}{\tau_2(k_\parallel)}\rho_{12}(k_\parallel,t)+\frac{ie}{\hbar}\mathbf{E}_L(t)\cdot\mathbf{r}_{12}(\mathbf{k}_\parallel)[\rho_{22}(k_\parallel,t)-\rho_{11}(k_\parallel,t)]+\frac{ie}{\hbar}\mathbf{E}_L(t)\cdot\mathbf{r}_{13}(\mathbf{k}_\parallel)$$
$$\times\rho_{23}^*(k_\parallel,t)-\beta_{21,13}[\Omega_{31}(k_\parallel)]\rho_{13}(k_\parallel,t), \tag{37}$$

$$\frac{d}{dt}\rho_{13}(k_\parallel,t)=i\Omega_{31}(k_\parallel)\rho_{13}(k_\parallel,t)-\frac{1}{\tau_3(k_\parallel)}\rho_{13}(k_\parallel,t)+\frac{ie}{\hbar}\mathbf{E}_L(t)\cdot\mathbf{r}_{13}(\mathbf{k}_\parallel)[\rho_{33}(k_\parallel,t)-\rho_{11}(k_\parallel,t)]$$
$$+\frac{ie}{\hbar}\mathbf{E}_L(t)\cdot\mathbf{r}_{12}(\mathbf{k}_\parallel)\rho_{23}(k_\parallel,t)-\beta_{31,12}[\Omega_{31}(k_\parallel)]\rho_{12}(k_\parallel,t), \tag{38}$$

$$\frac{d}{dt}\rho_{23}(k_\parallel,t)=i\Omega_{32}\rho_{23}(k_\parallel,t)-\left[\frac{1}{\tau_2(k_\parallel)}+\frac{1}{\tau_3(k_\parallel)}\right]\rho_{23}(k_\parallel,t)+\frac{ie}{\hbar}\mathbf{E}_L(t)\cdot\mathbf{r}_{12}^*(\mathbf{k}_\parallel)$$
$$\times\rho_{13}(k_\parallel,t)-\frac{ie}{\hbar}\mathbf{E}_L(t)\cdot\mathbf{r}_{13}(\mathbf{k}_\parallel)$$
$$\times\rho_{12}^*(k_\parallel,t)+\beta_{23,23}[\Omega_{32}(k_\parallel)]\rho_{23}^*(k_\parallel,t)-\{\beta_{21,13}[\Omega_{31}(k_\parallel)]\rho_{33}(k_\parallel,t)+\beta_{31,12}[\Omega_{21}(k_\parallel)]\rho_{22}(k_\parallel,t)\}, \tag{39}$$

and for the closed system we have an additional restraint,

$$\frac{d\rho_{33}(k_\parallel,t)}{dt}=-\left[\frac{d\rho_{11}(k_\parallel,t)}{dt}+\frac{d\rho_{22}(k_\parallel,t)}{dt}\right].$$

If we only seek the steady-state solutions of Eqs. (35)–(39), we get the following set of algebraic equations:

$$2\beta_{21,12}[\Omega_{21}(k_\parallel)]\rho_{22}(k_\parallel)+2\beta_{31,13}[\Omega_{31}(k_\parallel)]\rho_{33}(k_\parallel)+\Omega_{12}^R(k_\parallel)\mathrm{Im}[\rho_{12}(k_\parallel)]+\Omega_{13}^R(k_\parallel)\mathrm{Im}[\rho_{13}(k_\parallel)]+2\{\beta_{31,12}[\Omega_{21}(k_\parallel)]$$
$$+\beta_{21,13}[\Omega_{31}(k_\parallel)]\}\mathrm{Re}[\rho_{23}(k_\parallel)]=0, \tag{40}$$

$$-\frac{2}{\tau_2(k_\parallel)}\rho_{22}(k_\parallel)+2\beta_{32,23}[\Omega_{32}(k_\parallel)]\rho_{33}(k_\parallel)-\Omega_{12}^R(k_\parallel)\mathrm{Im}[\rho_{12}(k_\parallel)]-2\beta_{21,13}[\Omega_{31}(k_\parallel)]\mathrm{Re}[\rho_{23}(k_\parallel)]=0, \tag{41}$$

$$i[\omega_L-\Omega_{21}(k_\parallel)]\rho_{12}(k_\parallel)=-\frac{1}{\tau_2(k_\parallel)}\rho_{12}(k_\parallel)+\frac{i\Omega_{12}^R(k_\parallel)}{2}[\rho_{22}(k_\parallel)-\rho_{11}(k_\parallel)]+\frac{i\Omega_{13}^R(k_\parallel)}{2}\rho_{23}^*(k_\parallel)-\beta_{21,13}[\Omega_{31}(k_\parallel)]\rho_{13}(k_\parallel), \tag{42}$$

$$i[\omega_L-\Omega_{31}(k_\parallel)]\rho_{13}(k_\parallel)=-\frac{1}{\tau_3(k_\parallel)}\rho_{13}(k_\parallel)+\frac{i\Omega_{13}^R(k_\parallel)}{2}[\rho_{33}(k_\parallel)-\rho_{11}(k_\parallel)]+\frac{i\Omega_{12}^R(k_\parallel)}{2}\rho_{23}(k_\parallel)-\beta_{31,12}[\Omega_{21}(k_\parallel)]\rho_{12}(k_\parallel), \tag{43}$$

$$i\Omega_{32}\rho_{23}(k_\parallel)-\left[\frac{1}{\tau_2(k_\parallel)}+\frac{1}{\tau_3(k_\parallel)}\right]\rho_{23}(k_\parallel)+\frac{i\Omega_{12}^R(k_\parallel)}{2}\rho_{13}(k_\parallel)-\frac{i\Omega_{13}^R(k_\parallel)}{2}\rho_{12}^*(k_\parallel)+\beta_{23,23}[\Omega_{32}(k_\parallel)]\rho_{23}^*(k_\parallel)$$
$$-\{\beta_{21,13}[\Omega_{31}(k_\parallel)]\rho_{33}(k_\parallel)+\beta_{31,12}[\Omega_{21}(k_\parallel)]\rho_{22}(k_\parallel)\}=0. \tag{44}$$

Here, for non-steady-state solutions in interband-coupled QW's, we have the initial condition

$$\rho_{11}^{(0)}(k_\parallel)=1, \quad \rho_{22}^{(0)}(k_\parallel)=\rho_{33}^{(0)}(k_\parallel)=0,$$

and $\rho_{jj'}^{(0)}(k_\parallel)=0$ for $j\neq j'$, where $1-\rho_{11}(k_\parallel)$ is the hole distribution function. In Eqs. (40)–(44), $\Omega_{ij}^{R}(k_\parallel)=2e\mathbf{E}_L^0\cdot\mathbf{r}_{ij}(\mathbf{k}_\parallel)/\hbar$ is the laser-field Rabi frequency, $|\mathbf{E}_L^0|$ is the amplitude of $\mathbf{E}_L(t)$, $1/\tau_2(k_\parallel)=\beta_{21,12}[\Omega_{21}(k_\parallel)]$, and $1/\tau_3(k_\parallel)=\beta_{31,13}[\Omega_{31}(k_\parallel)]+\beta_{32,23}[\Omega_{32}(k_\parallel)]$. For intersubband-coupled QW's, we have the following different initial condition:

$$\rho_{jj}^{(0)}(k_\parallel)=\theta[\mathcal{E}_j(k_\parallel)-\mathcal{E}_F] \quad \text{for} \quad j=1,2,3,$$

and $\rho_{jj'}^{(0)}(k_\parallel)=0$ for $j\neq j'$, where $\mathcal{E}_F$ is the Fermi energy of electrons at zero temperature. In this case, the resulting distributions $\rho_{jj}^{(0)}(k_\parallel)$ on different energy levels are uniform with respect to $k_\parallel$ since the electron energy-level separation and the envelope function are independent of $k_\parallel$. However, the distributions on different energy levels for interband-coupled QW's exhibit a peak with respect to $k_\parallel$.

In Eqs. (40) and (41), the terms $\Omega_{12}^{R}(k_\parallel)\mathrm{Im}[\rho_{12}(k_\parallel)]$ and $\Omega_{13}^{R}(k_\parallel)\mathrm{Im}[\rho_{13}(k_\parallel)]$ represent the stimulated electron transitions between the lower state and the upper doublet. In Eqs. (42) and (43), the terms $\beta_{21,13}[\Omega_{31}(k_\parallel)]\rho_{13}(k_\parallel)$ and $\beta_{31,12}[\Omega_{21}(k_\parallel)]\rho_{12}(k_\parallel)$ stand for the ODRDC, which is responsible for the quantum interference between the nearly resonant electron transitions from $|1\mathbf{k}_\parallel\rangle$ to $|2\mathbf{k}_\parallel\rangle$ and $|3\mathbf{k}_\parallel\rangle$. Finally, the terms $[i\Omega_{13}^{R}(k_\parallel)/2]\rho_{23}^{*}(k_\parallel)$ and $[i\Omega_{12}^{R}(k_\parallel)/2]\rho_{23}(k_\parallel)$ in Eqs. (42) and (43) come from the induced quantum coherence, i.e., $\rho_{23}(k_\parallel)\neq 0$.

B. Optical absorption and photoluminescence spectra

In order to explore the dynamical property of the coupled electron-photon states in the laser-coupled QW's, we need to apply a weak probe field $\mathbf{E}_P(t)$ to the system, delayed in time from the strong pump laser $\mathbf{E}_L(t)$. The frequency of the probe field is ω_P and the polarization of $\mathbf{E}_P(t)$ is set perpendicular to the z direction for interband pumping and parallel to the z direction for intersubband pumping. When $\mathbf{E}_P(t)$ is delayed in time properly with respect to $\mathbf{E}_L(t)$ and propagates in the direction slightly away from $\mathbf{E}_L(t)$, the transient probe signal can be utilized to analyze the time evolution of the electron and hole distributions on different energy levels in the QW's [17]. The standard probing techniques include time-resolved optical absorption and photoluminescence.

For the probe-field absorption process in the QW's, the linear absorption coefficient $\beta_P(\omega_P;t)$ at zero temperature is found to be [18]

$$\beta_P(\omega_P;t)=\frac{\omega_P}{cn_P(\omega_P;t)}\mathrm{Im}[\alpha_P(\omega_P;t)]. \tag{45}$$

The refractive-index function in Eq. (45) is

$$n_P(\omega_P;t)=\frac{1}{\sqrt{2}}\{\epsilon_r+\mathrm{Re}[\alpha_P(\omega_P;t)]+\sqrt{\{\epsilon_r+\mathrm{Re}[\alpha_P(\omega_P;t)]\}^2+\{\mathrm{Im}[\alpha_P(\omega_P;t)]\}^2}\}^{1/2}, \tag{46}$$

where $\alpha_P(\omega_P;t)$ in Eqs. (45) and (46) is the Lorentz ratio function given by [18]

$$\alpha_P(\omega_P;t)=-\left[\frac{\hbar}{2\epsilon_0 L_z\mathcal{S}|\mathbf{E}_P^0|^2}\right]\times\sum_{\mathbf{k}_\parallel}[\rho_{12}'(k_\parallel,\omega_P;t)\Omega_{21}^{P}(k_\parallel)+\rho_{13}'(k_\parallel,\omega_P;t)\Omega_{31}^{P}(k_\parallel)]. \tag{47}$$

Here, we denote the density-matrix elements associated with the strong $\mathbf{E}_L(t)$ field by $\rho_{jj'}(k_\parallel,t)$ and those associated with the weak $\mathbf{E}_P(t)$ field by $\rho_{jj'}'(k_\parallel,\omega_P;t)$. L_z in Eq. (47) is the total well width of the RADQW's including the thin middle barrier thickness. In Eq. (47), $|\mathbf{E}_P^0|$ is the amplitude of $\mathbf{E}_P(t)$, $\Omega_{ij}^{P}(k_\parallel)=2e\mathbf{E}_P^0\cdot\mathbf{r}_{ij}(\mathbf{k}_\parallel)/\hbar$, and $\rho_{12}'(k_\parallel,\omega_P;t)$ and $\rho_{13}'(k_\parallel,\omega_P;t)$ in Eq. (47) are determined from the following pair of coupled equations:

$$\left\{i[\omega_P-\Omega_{21}(k_\parallel)]+\frac{1}{\tau_2(k_\parallel)}\right\}\rho_{12}'(k_\parallel,\omega_P;t)+\beta_{21,13}[\Omega_{31}(k_\parallel)]\rho_{13}'(k_\parallel,\omega_P;t)=\frac{i}{2}\Omega_{12}^{P}(k_\parallel)[\rho_{22}(k_\parallel,t)-\rho_{11}(k_\parallel,t)]+\frac{i}{2}\Omega_{13}^{P}(k_\parallel)\rho_{23}^{*}(k_\parallel,t), \tag{48}$$

$$\beta_{31,12}[\Omega_{21}(k_\parallel)]\rho_{12}'(k_\parallel,\omega_P;t)+\left\{i[\omega_P-\Omega_{31}(k_\parallel)]+\frac{1}{\tau_3(k_\parallel)}\right\}\rho_{13}'(k_\parallel,\omega_P;t)=\frac{i}{2}\Omega_{13}^{P}(k_\parallel)[\rho_{33}(k_\parallel,t)-\rho_{11}(k_\parallel,t)]+\frac{i}{2}\Omega_{12}^{P}(k_\parallel)\rho_{23}(k_\parallel,t). \tag{49}$$

Here, the difference of occupation probabilities $\rho_{jj}(k_\parallel,t)-\rho_{11}(k_\parallel,t)$ for $j=2,3$ in Eqs. (48) and (49) contains the effect of *transition blocking*, namely $\rho_{22}(k_\parallel,t),\rho_{33}(k_\parallel,t)\neq 0$ due to laser excitation. The terms containing $\rho_{23}(k_\parallel,t)$ or $\rho_{23}^*(k_\parallel,t)$ come from induced quantum coherence due to laser pumping, which directly modifies the difference of occupation probabilities. The coupling terms $\beta_{21,13}[\Omega_{31}(k_\parallel)]\rho'_{13}(k_\parallel,\omega_P;t)$ and $\beta_{31,12}[\Omega_{21}(k_\parallel)]\rho'_{12}(k_\parallel,\omega_P;t)$ correspond to the ODRDC between the two nearly resonant optical transitions from $\mathcal{E}_1(\mathbf{k}_\parallel)$ to $\mathcal{E}_2(\mathbf{k}_\parallel)$ and $\mathcal{E}_3(\mathbf{k}_\parallel)$.

For the optical absorption of the strong pump-laser field, the absorption coefficient $\beta_L(\omega_L;t)$ can be obtained from Eq. (45) by replacing ω_P, $n_P(\omega_P;t)$, and $\alpha_P(\omega_P;t)$ with ω_L, $n_L(\omega_L;t)$, and $\alpha_L(\omega_L;t)$. Here, $n_L(\omega_L;t)$ can be calculated from Eq. (46) by replacing $\alpha_P(\omega_P;t)$ with $\alpha_L(\omega_L;t)$, and $\alpha_L(\omega_L;t)$ is given by

$$\alpha_L(\omega_L;t)=-\left[\frac{\hbar}{2\epsilon_0 L_z\mathcal{S}|\mathbf{E}_L^0|^2}\right]\langle\Omega_L^R(t)\rangle, \tag{50}$$

where the quantum-statistical average of the laser-field Rabi frequency is

$$\langle\Omega_L^R(t)\rangle=\sum_{j<j'}\sum_{\mathbf{k}_\parallel}\rho_{jj'}(k_\parallel,t)\Omega_{j'j}^R(k_\parallel), \tag{51}$$

which includes the coherent contribution $\rho_{23}(k_\parallel,t)\Omega_{32}^R(k_\parallel)$. $\alpha_L(\omega_L;t)$ in Eq. (50) is found depending on $\mathbf{E}_L^0$. It indicates a nonlinear absorption process for the pump-laser field.

For photoluminescence in the QW's pumped by a laser, the spectroscopy is determined by the following spontaneous rate [19]:

$$\begin{aligned}R_{\rm sp}(\omega_e;t)=&\left[\frac{2\sqrt{\epsilon_r}e^2\omega_e}{\pi^2\hbar^2\epsilon_0 c^3 L_z\mathcal{S}}\right]\sum_{j=2}^{3}\sum_{\mathbf{k}_\parallel}\rho_{jj}(k_\parallel,t)\\&\times[1-\rho_{11}(k_\parallel,t)]Q_{1,j}(k_\parallel)\\&\times\left\{\frac{1/\tau_j(k_\parallel)}{[1/\tau_j(k_\parallel)]^2+[\omega_e-\Omega_{j1}(k_\parallel)]^2}\right\},\end{aligned} \tag{52}$$

where ω_e is the frequency of the emitted photons, and the form factor is given by

$$Q_{1,j}(k_\parallel)=\left|\frac{\mathbf{w}_e\cdot\hat{\mathbf{p}}_{1j}}{m_0}\right|^2=\begin{cases}(1/\hbar^2)\left|\displaystyle\int_{-\infty}^{+\infty}dzF_{1k_\parallel}^*(z)P_0(z)F_{jk_\parallel}(z)\right|^2 & \text{for interband pumping}\\ \omega_e^2\left|\displaystyle\int_{-\infty}^{+\infty}dzF_{1k_\parallel}^*(z)zF_{jk_\parallel}(z)\right|^2 & \text{for intersubband pumping.}\end{cases} \tag{53}$$

Here, $\mathbf{w}_e$ in Eq. (53) is the unit polarization vector, and $F_{1k_\parallel}(z)$ and $F_{jk_\parallel}(z)$ are the single-band z-component parts of the envelope functions in Eq. (A16) after neglecting the band mixing. The spontaneous emission is polarized within the QW plane for interband pumping and polarized in the z direction for intersubband pumping.

VI. NUMERICAL RESULTS AND DISCUSSIONS

In this section, we limit ourselves to the steady-state case, and only a RADQW sample with intersubband laser pumping will be considered as an example. We first present the numerical results for the laser-field absorption in this RADQW. The effects of the transition blocking, power broadening, and quantum interference are observed in the calculated absorption spectrum. The influences of the tunneling gap, off-resonance, and momentum-dependent energy-level separation to the laser-field absorption are also studied. After this, the spectra of the probe-field absorption are displayed for the RADQW's selectively coupled by a laser field. The optical gain of the probe field is found as a result of the partial momentum-space inversion of the subband occupation probability. Finally, the effects of the transition blocking, induced quantum coherence, and ODRDC on the probe-field absorption are investigated.

The sample used in our numerical study is a doped RADQW, as shown in Fig. 1(b). The barrier material is $Al_{0.35}Ga_{0.65}As$ and the materials for the left and right QW's are GaAs and $Al_{0.208}Ga_{0.792}As$, respectively. The donors in the left QW are assumed completely ionized, giving rise to

TABLE I. Conduction-band offsets $\Delta E_{C1}/\Delta E_{C2}$, step height ΔU, well widths L_{W1}/L_{W2}, middle barrier thickness L_B, electron density n_{2D}, and average dielectric constant ϵ_r for the sample shown in Fig. 1(b).

$\Delta E_{C1}/\Delta E_{C2}$ (meV)	ΔU (meV)	L_{W1}/L_{W2} (Å)	L_B (Å)	n_{2D} (10^{11} cm^{-2})	ϵ_r
249/101	148	75/85	50	1.6	11.73

TABLE II. Calculated electron energy levels E_1^L and E_2^L in the left QW and E_1^R and E_2^R in the right QW for the sample shown in Fig. 1(b).

E_1^L (meV)	E_2^L (meV)	E_1^R (meV)	E_2^R (meV)
45	173	173	237

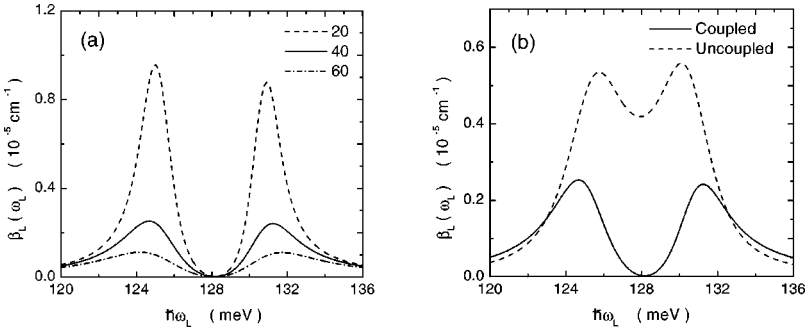

FIG. 2. $\beta_L(\omega_L)$ for the sample shown in Fig. 1(b) as a function of $\hbar\omega_L$. In (a), $\beta_L(\omega_L)$ is presented for different $|\mathbf{E}_L^0| = 20$, 40, and 60 kV/cm. In (b), a comparison of $\beta_L(\omega_L)$ is made at $|\mathbf{E}_L^0| = 40$ kV/cm with (coupled) and without (uncoupled) the ODRDC.

an electron density n_{2D}. There are two confined electron states in each QW, represented by E_1^L and E_2^L in the left and E_1^R and E_2^R in the right. The sample parameters and the calculated energy levels in the left and right QW's are summarized in Tables I and II. The upper energy level in the left QW is aligned with the lower energy level in the right QW, producing a tunneling-split doublet. The external laser and probe fields applied to the system are all polarized in the z direction. The frequency of the laser field is set close to the energy separation between the lower level in the left QW and the doublet. As a result, the above three-level model for the intersubband-coupled QW's can be directly applied.

A. Absorption of pump-laser field

Figure 2 shows the steady-state laser-field absorption coefficient $\beta_L(\omega_L)$ as a function of the laser photon energy $\hbar\omega_L$. In (a), we find $\beta_L(\omega_L)$ with different laser-field strengths $|\mathbf{E}_L^0| = 20$, 40, and 60 kV/cm, and in (b) we show the comparison of $\beta_L(\omega_L)$ with (coupled) and without (uncoupled) ODRDC at $|\mathbf{E}_L^0| = 40$ kV/cm. The increase of $|\mathbf{E}_L^0|$ pumps more electrons into the upper doublet, reducing the occupation probability of initial states and the availability of final states at the same time for the absorption process. This gives rise to a smaller $\beta_L(\omega_L)$ as $|\mathbf{E}_L^0|$ increases. Moreover, the power broadening of the two absorption peaks also increases with $|\mathbf{E}_L^0|$, which further brings down the peak strengths. The most interesting feature seen in (a) is the zero absorption in the overlapping region of the two peaks. This is a direct result of the quantum interference between the two optical transitions associated with two peaks separated by a small tunneling gap. It is described by the two last terms in Eqs. (42) and (43). The influence of the quantum interference can be clearly seen in (b) through a comparison of $\beta_L(\omega_L)$ with and without these two terms, where the zero absorption disappears and the two enhanced absorption peaks become strongly overlapped to form a very weak minimum in the middle whenever the ODRDC is excluded. Only when ODRDC is included can the zero absorption appear at the middle of the tunneling gap.

In order to elucidate the physics of quantum interference, we calculate the statistically averaged transition dipole moment as a function of $\hbar\omega_L$,

$$\langle \Omega_{ij}^R \rangle = \left| \sum_{\mathbf{k}_\parallel} \rho_{ij}(k_\parallel) \Omega_{ij}^R \right| ,$$

which gives $\langle \Omega_L^R \rangle = \Sigma_{i<j} \langle \Omega_{ij}^R \rangle$ in Eq. (51), where $i<j = 1,2,3$ and $\langle \Omega_{ij}^R \rangle$ is independent of $k_\parallel$ for the intersubband-coupled RADQW's. In Fig. 3, scaled $\langle \Omega_{12}^R \rangle$ and $\langle \Omega_{13}^R \rangle$ at $|\mathbf{E}_L^0| = 40$ kV/cm display minima at the two absorption peak positions in Fig. 2, even though the imaginary parts of $\langle \Omega_{12}^R \rangle$ and $\langle \Omega_{13}^R \rangle$ reach the maximum in $\langle \Omega_{12}^R \rangle$ and $\langle \Omega_{13}^R \rangle$ at the two peak positions. Furthermore, we find that

$$\langle \Omega_{12}^R + \Omega_{13}^R \rangle = \left| \sum_{\mathbf{k}_\parallel} [\rho_{12}(k_\parallel)\Omega_{12}^R + \rho_{13}(k_\parallel)\Omega_{13}^R] \right| \neq \langle \Omega_{12}^R \rangle + \langle \Omega_{13}^R \rangle$$

reaches a minimum around the middle of the tunneling gap due to the phase cancellation between $\langle \Omega_{12}^R \rangle$ and $\langle \Omega_{13}^R \rangle$, which is termed quantum interference between the two optical transitions. The finite value of $\langle \Omega_{23}^R \rangle$ is due to the induced quantum coherence by the laser field, i.e., $\rho_{23}(k_\parallel) \neq 0$ as $|\mathbf{E}_L^0| \neq 0$, and the phase cancellation is not seen in the induced quantum coherence. The induced quantum coherence will modify the difference of the occupation probabilities, as can be seen from Eqs. (42) and (43).

In Fig. 4, we display the calculated laser-field refractive-index function $n_L(\omega_L)$ in (a) for different $|\mathbf{E}_L^0| = 20$, 40, and 60 kV/cm, and the comparison of $n_L(\omega_L)$ in (b) with (coupled) and without (uncoupled) ODRDC at $|\mathbf{E}_L^0| = 60$ kV/cm. With the increase of $|\mathbf{E}_L^0|$, the dynamical range

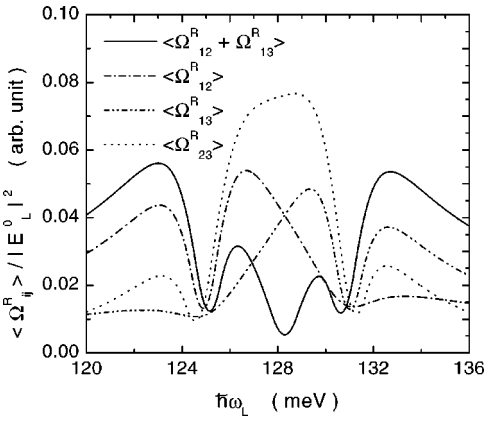

FIG. 3. $\langle \Omega_{ij}^R \rangle / |\mathbf{E}_L^0|^2$ with $i<j = 1,2,3$ for the sample shown in Fig. 1(b) as a function of $\hbar\omega_L$ at $|\mathbf{E}_L^0| = 40$ kV/cm. $\langle \Omega_{12}^R + \Omega_{13}^R \rangle$ exhibits a quantum interference by showing a minimum at the middle of the tunneling gap.

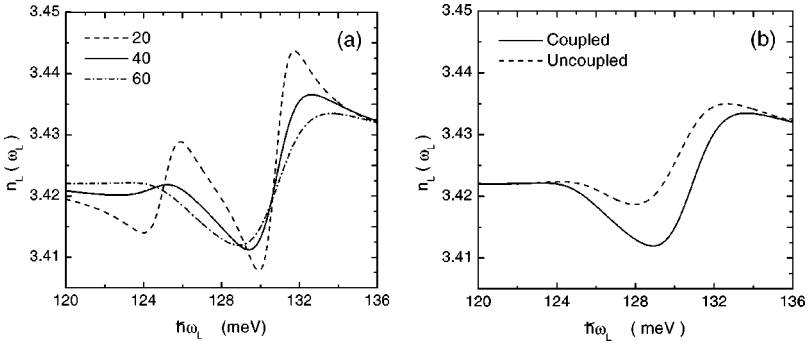

FIG. 4. $n_L(\omega_L)$ for the sample shown in Fig. 1(b) as a function of $\hbar\omega_L$. In (a), $n_L(\omega_L)$ is displayed for $|\mathbf{E}_L^0|=20$, 40, and 60 kV/cm. In (b), a comparison of $n_L(\omega_L)$ is shown at $|\mathbf{E}_L^0|=60$ kV/cm with (coupled) and without (uncoupled) the ODRDC.

$n_L(\omega_L)-\sqrt{\epsilon_r}$ ($\sqrt{\epsilon_r}=3.425$) is reduced due to the lack of empty final states and occupied initial states in the absorption process. The dynamical range becomes very small at the two absorption peaks. The influence of ODRDC between the two nearly degenerate optical transitions in the RADQW's is found appreciable in (b), where the negative (positive) dynamical range of $n_L(\omega_L)$ is enhanced (suppressed) by ODRDC, respectively. No unique feature of the quantum interference is seen in $n_L(\omega_L)$.

Figure 5 is devoted to the scaled ground-subband electron density, defined by

$$\frac{n_1}{n_{2D}}=\frac{2}{N_e}\sum_{\mathbf{k}_\parallel}\rho_{11}(k_\parallel),$$

where N_e is the total number of electrons in the RADQW's. The calculated n_1/n_{2D} is shown in (a) as a function of $\hbar\omega_L$ for various $|\mathbf{E}_L^0|=20$, 40, and 60 kV/cm and in (b) for the comparison of n_1/n_{2D} with (coupled) and without (uncoupled) ODRDC at $|\mathbf{E}_L^0|=40$ kV/cm. The two minima in (a) originate from the resonant excitation of electrons from the ground level to the upper doublet. As $|\mathbf{E}_L^0|$ increases, the two minima become deeper due to the fact that more electrons are pumped to the upper doublet. Meanwhile, these two minima become broader because of the power-broadening effect, making the maximum between these two minima shallower as a result of the overlap between these two minima. Each minimum approximately reaches a value of $\frac{1}{2}$, a strong-field limit for a single minimum, at $|\mathbf{E}_L^0|=20$ kV/cm since these two minima are relatively nonoverlapping. However, when they begin overlapping with increased $|\mathbf{E}_L^0|$, the minimum of n_1/n_{2D} can go below $\frac{1}{2}$. The effect of quantum interference can be clearly seen in (b), where the maximum between the two minima is greatly enhanced by turning on ODRDC, which suppresses the overlap between the two minima in the absence of ODRDC and reduces the power-broadening effect at the same time. This provides us with a tool for freezing the electrons to the ground state by setting $\hbar\omega_L$ within the tunneling gap.

In Fig. 6, we check the influences of the electron tunneling and off-resonance on $\beta_L(\omega_L)$ at $|\mathbf{E}_L^0|=40$ kV/cm. With the reduction of the middle-barrier thickness from 60 Å down to 40 Å in (a), the separation of the two absorption peaks becomes larger due to the enhanced electron tunneling. However, the strength of the absorption peaks and the peak broadening remains constant since both the transition-blocking and power-broadening effects are not changed for fixed $|\mathbf{E}_L^0|$. When the alloy-composition index x_c of the right QW is varied from 20.8% to 19.8% (21.8%) in (b), the energy level E_1^R in the right QW shifts down (up) with respect to the energy level E_1^L in the left QW. When $x_c=19.8\%$ is chosen, the energy separation from $|1\mathbf{k}_\parallel\rangle$ to $|2\mathbf{k}_\parallel\rangle$ is reduced, and the lower intrawell transition peak at $x_c=20.8\%$ switches to the interwell one and greatly decreases its strength. But the upper peak strength is increased because of the enhancement of the overlap of electron wave functions in the left QW. Both the lower and upper absorption peaks are shifted down due to, respectively, the reduction of $\Omega_{21}(k_\parallel)$ and the decreased electron tunneling, which pulls the upper level of the doublet down. Similarly, when $x_c=21.8\%$ is used, the energy separation from $|1\mathbf{k}_\parallel\rangle$ to $|3\mathbf{k}_\parallel\rangle$ is increased, and the switching of the upper intrawell peak at $x_c=20.8\%$ to the interwell one happens again. Consequently, this gives rise to the upward shifts of both absorption peaks and the reduced (increased) strengths of the upper (lower) absorption peaks. In each of these cases, the laser frequency for zero absorption moves away from the middle of the tunneling gap [2]. The off-resonant effect above can also be produced by

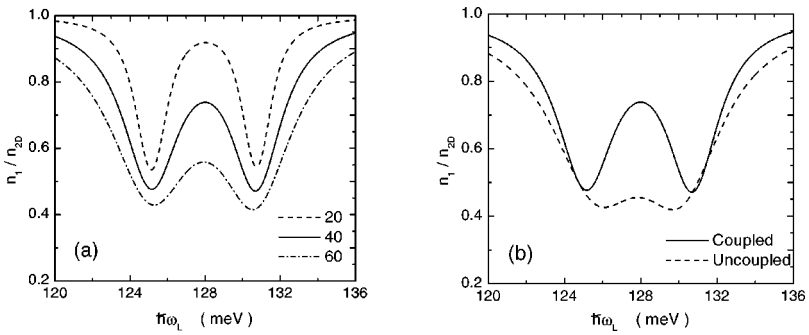

FIG. 5. n_1/n_{2D} for the sample shown in Fig. 1(b) as a function of $\hbar\omega_L$. In (a), n_1/n_{2D} is shown for $|\mathbf{E}_L^0|=20$, 40, and 60 kV/cm. In (b), a comparison of n_1/n_{2D} is exhibited at $|\mathbf{E}_L^0|=40$ kV/cm with (coupled) and without (uncoupled) the ODRDC.

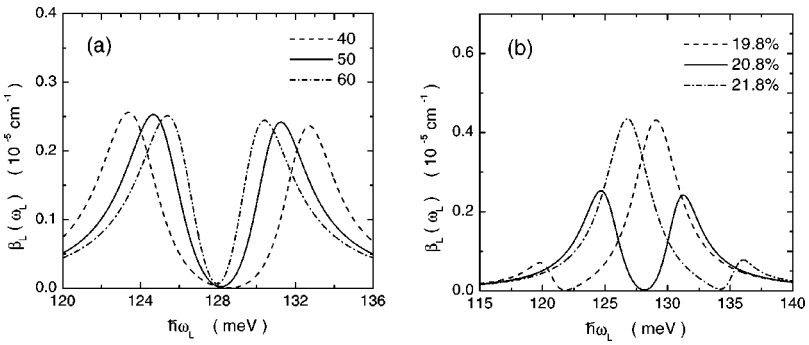

FIG. 6. $\beta_L(\omega_L)$ for the sample shown in Fig. 1(b) as a function of $\hbar\omega_L$. In (a), $\beta_L(\omega_L)$ is presented for $L_B=40$, 50, and 60 Å at $|\mathbf{E}_L^0|=40$ kV/cm. In (b), $\beta_L(\omega_L)$ is given for different right-well alloy-composition indexes $x_c=19.8\%$, 20.8%, and 21.8% at $|\mathbf{E}_L^0|=40$ kV/cm.

applying a small dc bias field in the z direction, which enables us to tune the zero-absorption laser frequency within the tunneling gap.

For the $Al_xGa_{1-x}As/GaAs$ QW structure, the electron effective mass in the $Al_xGa_{1-x}As$ barrier layer is larger than that in the GaAs well layer. Therefore, the electrons with higher energies have a larger effective mass than those with lower energies because the wave function can penetrate into the outer barriers more efficiently. This introduces a $k_\parallel$-dependent energy-level separation. As a result, the energy separation between the lower and upper subbands becomes smaller as $k_\parallel$ moves away from zero. Moreover, we know that the optical absorption is the sum over all possible vertical transitions from different occupied initial $k_\parallel$ states in the current case. Consequently, a large broadening of the absorption peak is expected for the QW's with high n_{2D} (more occupied initial $k_\parallel$ states). From Fig. 7(a), we see the increase of the broadening of the absorption peaks with n_{2D} and the development of the low-energy tail of $\beta_L(\omega_L)$ due to high-$k_\parallel$ transitions at $|\mathbf{E}_L^0|=40$ kV/cm. The zero absorption at the middle of the tunneling gap disappears as n_{2D} increases. We know that the wave function of the lower level in the doublet has a maximum distribution around the middle barrier region of the RADQW's. This results in a large effective-mass change in the lower level compared to that in the upper level of the doublet. This effect is seen as the small downward shift of the upper absorption peak compared to that of the lower absorption peak. The effect of the $k_\parallel$-dependent energy-level separation can also be seen from n_1/n_{2D} in (b), where the depth of the two minima is greatly reduced with increased n_{2D} and the low-energy tail of n_1/n_{2D} is gradually developed. In the presence of a large $k_\parallel$-dependent energy-level separation, quantum interference between the two electron transitions is completely destroyed. The maximum in (a) and the minimum in (b) for $n_{2D}=1.6\times10^{12}$ cm^{-2} originate from the strong overlap of the two broadened peaks.

B. Absorption of probe field

Figure 8 shows the linear probe-field absorption coefficient $\beta_P(\omega_P)$ and refractive-index function $n_P(\omega_P)$, which are independent of probe-field strength, as a function of the probe photon energy $\hbar\omega_P$ at $|\mathbf{E}_L^0|=40$ kV/cm. We find a lot of changes from $\beta_P(\omega_P)$ and $n_P(\omega_P)$ in (a) and (b) for different values of $\hbar\omega_L=125.0$, 128.1, and 130.8 meV. From (a), we see a hole in the very weak lower absorption peak (a ''split'' peak) associated with the transition from $|1\mathbf{k}_\parallel\rangle$ to $|2\mathbf{k}_\parallel\rangle$ for $\hbar\omega_L=125.0$ meV and a strong higher absorption peak associated with the transition from $|1\mathbf{k}_\parallel\rangle$ to $|3\mathbf{k}_\parallel\rangle$. However, when $\hbar\omega_L=130.8$ meV, we observe a strong lower absorption peak and a weak higher absorption peak that exhibits a hole. At $\hbar\omega_L=128.1$ meV, only two strong absorption peaks exist and no hole in either of them is seen. The occurrence of the hole in each weak absorption peak is due to the optical gain for the probe field in the QW's selectively pumped by a laser. From (b), we find a large dynamical range in $n_P(\omega_P)-\sqrt{\epsilon_r}$ with $\sqrt{\epsilon_r}=3.425$ wherever there is a strong absorption peak.

To uncover the physics behind the probe-field optical gain in Fig. 8(a), we present in Fig. 9 the difference of the occupation probabilities $\rho_{11}(k_\parallel)-\rho_{jj}(k_\parallel)$ for $j=2,3$ at $|\mathbf{E}_L^0|=40$ kV/cm as a function of the electron wave vector $k_\parallel$. When $\hbar\omega_L=125.0$ meV, we see from (a) that $\rho_{11}(k_\parallel)-\rho_{22}(k_\parallel)$ becomes negative for certain values of $k_\parallel$ as a result of the partial inversion of the occupation probability by the pump-laser excitation. Because of the $k_\parallel$-dependent energy-level separation, $\rho_{11}(k_\parallel)-\rho_{22}(k_\parallel)$ depends on $k_\parallel$ in

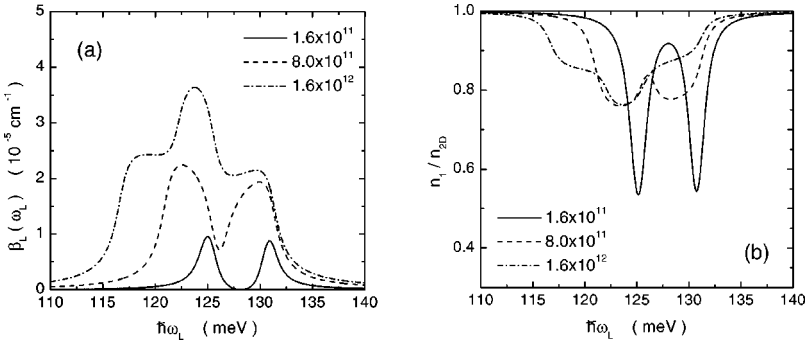

FIG. 7. $\beta_L(\omega_L)$ and n_1/n_{2D} for the sample shown in Fig. 1(b) as a function of $\hbar\omega_L$. In (a), $\beta_L(\omega_L)$ is displayed for $n_{2D}=1.6$, 8, and 16 $\times10^{11}$ cm^{-2} at $|\mathbf{E}_L^0|=40$ kV/cm. In (b), n_1/n_{2D} are compared for these three electron densities at 40 kV/cm.

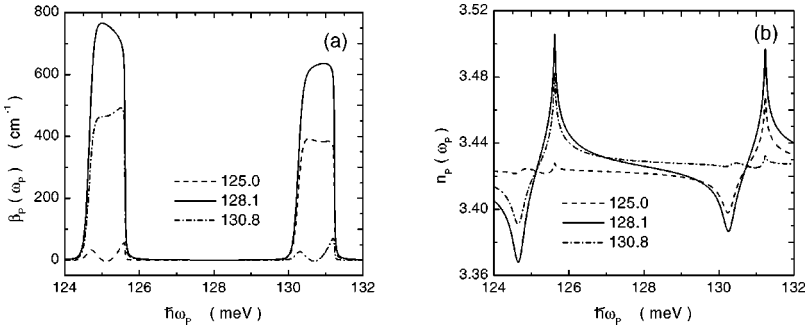

FIG. 8. $\beta_P(\omega_P)$ and $n_P(\omega_P)$ for the sample shown in Fig. 1(b) as a function of $\hbar\omega_P$ at $|\mathbf{E}_L^0| = 40$ kV/cm. $\beta_P(\omega_P)$ and $n_P(\omega_P)$ in (a) and (b) are presented for $\hbar\omega_L = 125.0$, 128.1, and 130.8 meV.

the range of $k_\parallel < k_F$, where k_F is the Fermi wave vector. The $k_\parallel$-dependent energy-level separation $\Omega_{21}(k_\parallel)$, which satisfies $\Omega_{21}(k_F) < \Omega_{21}(k_\parallel) < \Omega_{21}(0)$, causes a broadened absorption peak at $\hbar\omega_P = \Omega_{21}(k_\parallel)$ in Fig. 8(a). The optical gain occurs within this broadened peak for those $k_\parallel$ values satisfying $\hbar\omega_L = \Omega_{21}(k_\parallel)$ and producing partial inversion of the occupation probabilities. Similarly, we find from (b) that $\rho_{11}(k_\parallel) - \rho_{33}(k_\parallel)$ also becomes negative in a finite $k_\parallel$ region for $\hbar\omega_L = 130.8$ meV, which is associated with the optical gain in the upper absorption peak in Fig. 8(a). Finally, we know from (a) and (b) that there is no partial inversion for both $\rho_{11}(k_\parallel) - \rho_{22}(k_\parallel)$ and $\rho_{11}(k_\parallel) - \rho_{33}(k_\parallel)$ as $\hbar\omega_L = 128.1$ meV, which agrees with the two strong absorption peaks observed in Fig. 8(a).

From Eqs. (48) and (49), we know that the induced quantum coherence can have an affect on $\beta_P(\omega_P)$ by directly modifying the difference of the occupation probabilities, namely $\rho_{11}(k_\parallel) - \rho_{22}(k_\parallel)$ for the lower peak and $\rho_{11}(k_\parallel) - \rho_{33}(k_\parallel)$ for the upper peak, which appears as the terms containing $\rho_{23}(k_\parallel, t)$ and $\rho_{23}^*(k_\parallel, t)$. Moreover, the effect of ODRDC also affects $\beta_P(\omega_P)$ by changing this difference through the coupling between the two nearly resonant optical transitions, which is represented by the terms containing $\beta_{21,13}[\Omega_{31}(k_\parallel)]$ and $\beta_{31,12}[\Omega_{21}(k_\parallel)]$ in Eqs. (48) and (49). We compare $\beta_P(\omega_P)$ in Fig. 10 at $|\mathbf{E}_L^0| = 40$ kV/cm for four different cases. They are distinguished by including (coherent) or excluding (incoherent) the induced quantum coherence and by considering (coupled) or neglecting (uncoupled) ODRDC. In Figs. 10(a) and 10(b), we show $\beta_P(\omega_P)$ for $\hbar\omega_L = 125.0$ and 128.1 meV, respectively, where one can visualize the affect of induced quantum coherence by comparing the dash-dotted and dotted curves, or the affect of ODRDC by comparing the dashed and dotted curves. The full-theory result is represented by the solid curve. Appreciable change due to the induced quantum coherence and ODRDC is seen in (a) at $\hbar\omega_L = 125.0$ meV from both the higher strong absorption peak and the optical gain in the lower weak absorption peak. For the induced quantum coherence (dash-dotted and dotted curves), it slightly compensates for the partial inversion produced by the pump laser and reduces the difference of the occupation probabilities at $k_\parallel = 0$ as seen from the drop of the upper edges of the two absorption peaks. For the ODRDC (dashed and dotted curves), it greatly enhances the partial inversion of the occupation probability at $\hbar\omega_P = 125.0$ meV but slightly decreases the difference of the occupation probabilities at $\hbar\omega_P = 130.8$ meV shown as a deep hole in the lower peak and the drop of the upper edge of the higher peak. The full theory (solid curve) predicts a much shallower hole in the lower weak absorption peak as a combination of the contributions from both induced quantum coherence and ODRDC. When $\hbar\omega_L = 128.1$ meV, the induced quantum coherence reaches its maximum as seen from Fig. 3, and then increases the difference of the occupation probabilities at this time for both optical transitions. Similarly, the ODRDC also increases this difference at $\hbar\omega_L = 128.1$ meV. Consequently, a large increase of the absorption peak strength is observed for both optical transitions in (b) due to the constructive contributions from induced quantum coherence and ODRDC.

Figure 11 presents comparisons of $\beta_P(\omega_P)$ as a function of $\hbar\omega_P$ for $\hbar\omega_L = 130.8$ meV. We display $\beta_P(\omega_P)$ in (a) with different $|\mathbf{E}_L^0| = 20$, 40, and 60 kV/cm, and the affects of the induced quantum coherence and ODRDC in (b) at $|\mathbf{E}_L^0| = 60$ kV/cm. From (a), we find the increase of optical gain with $|\mathbf{E}_L^0|$ for the transition between states $|1\mathbf{k}_\parallel\rangle$ and $|3\mathbf{k}_\parallel\rangle$ due to the enhanced partial inversion of the electron occupation probability. Meanwhile, the strength of the lower absorption peak for the transition between states $|1\mathbf{k}_\parallel\rangle$ and $|2\mathbf{k}_\parallel\rangle$ decreases with $|\mathbf{E}_L^0|$ as a result of the transition-

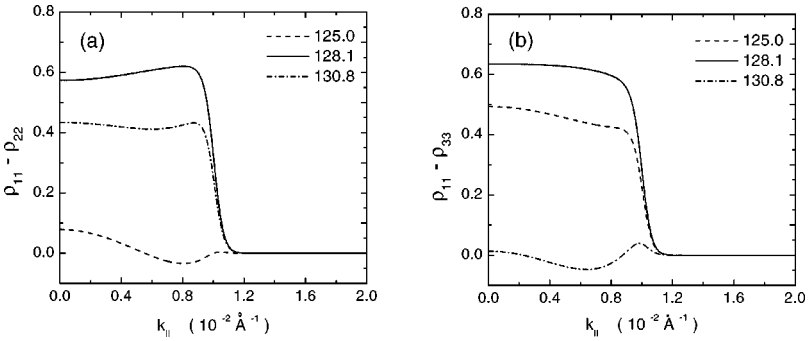

FIG. 9. $\rho_{11}(k_\parallel) - \rho_{jj}(k_\parallel)$ with $j = 2,3$ for the sample shown in Fig. 1(b) as a function of $k_\parallel$ at $|\mathbf{E}_L^0| = 40$ kV/cm. $\rho_{11}(k_\parallel) - \rho_{22}(k_\parallel)$ and $\rho_{11}(k_\parallel) - \rho_{33}(k_\parallel)$ are, respectively, displayed in (a) and (b) for $\hbar\omega_L = 125.0$, 128.1, and 130.8 meV.

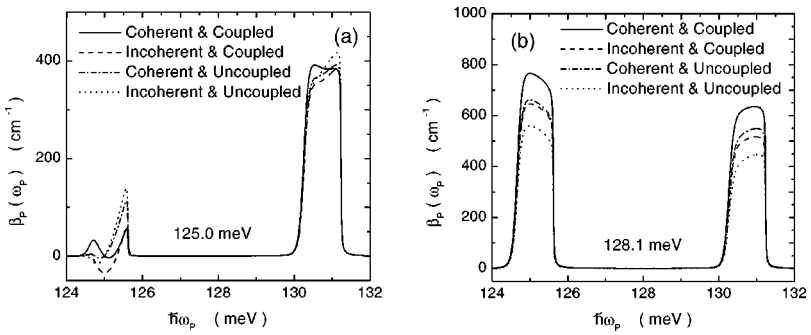

FIG. 10. $\beta_P(\omega_P)$ for the sample shown in Fig. 1(b) as a function of $\hbar\omega_P$ at $|\mathbf{E}_L^0|=40$ kV/cm in (a) and (b) for $\hbar\omega_L=125.0$ and 128.1 meV, respectively. In (a) and (b), $\beta_P(\omega_P)$ is computed for four different cases. They are (i) with both induced quantum coherence and ODRDC (coherent and coupled); (ii) without induced quantum coherence but with ODRDC (incoherent and coupled); (iii) with induced quantum coherence but without ODRDC (coherent and uncoupled); (iv) with neither induced quantum coherence nor ODRDC (incoherent and uncoupled).

blocking effect. From (b), we find an appreciable influence from the combined affects of induced quantum coherence and ODRDC on both the lower strong and higher weak absorption peaks. The induced quantum coherence (dash-dotted curve) is found to lower the strength of the lower absorption peak. When $\hbar\omega_P=130.8$ meV, the partial inversion of the occupation probability is greatly enhanced by the ODRDC (dashed curve). However, the difference of the occupation probabilities $\rho_{11}(k_\parallel)-\rho_{22}(k_\parallel)$ at $\hbar\omega_P=125.0$ meV decreases slightly. The optical gain of the probe field at $\hbar\omega_P=130.8$ meV is somewhat compensated by the induced quantum coherence (dash-dotted curve), which tends to reduce the partial inversion existing in the difference of the occupation probabilities between states $|1\mathbf{k}_\parallel\rangle$ and $|3\mathbf{k}_\parallel\rangle$. This leads to a very weak hole (solid curve) in the higher absorption peak.

In order to further explore the increase of the optical gain with $|\mathbf{E}_L^0|$ in Fig. 11(a), we present in Fig. 12 the difference of the occupation probabilities $\rho_{11}(k_\parallel)-\rho_{jj}(k_\parallel)$ for $j=2,3$ at $\hbar\omega_L=130.8$ meV with $|\mathbf{E}_L^0|=20$, 40, and 60 kV/cm as a function of $k_\parallel$. In (a), for the whole range of $|\mathbf{E}_L^0|$ considered, we do not see any negative difference of the occupation probabilities $\rho_{11}(k_\parallel)-\rho_{22}(k_\parallel)$. This agrees with the lower strong absorption peak observed for the transition between $|1\mathbf{k}_\parallel\rangle$ and $|2\mathbf{k}_\parallel\rangle$ in Fig. 11(a). However, we do find in Fig. 11(b) a negative region for $\rho_{11}(k_\parallel)-\rho_{33}(k_\parallel)$ at certain $k_\parallel$ values. The negative $k_\parallel$ region expands with $|\mathbf{E}_L^0|$, which explains the increase of the optical gain with $|\mathbf{E}_L^0|$ for the transition between $|1\mathbf{k}_\parallel\rangle$ and $|3\mathbf{k}_\parallel\rangle$.

VII. CONCLUSIONS AND REMARKS

In conclusion, we have derived the density-matrix equations in the presence of a pump-laser field for electrons in QW's by working in second quantization and including the off-diagonal radiative-decay coupling between a pair of electron transitions. These fully quantized density-matrix equations allow us to calculate simultaneously the time-dependent optical response of electrons and radiative decay of excited-state electrons quantum electrodynamically. On the basis of the derived density-matrix equations, the time-resolved photoluminescence spectrum of the system has been formulated. When another delayed weak probe field is applied, the time-resolved absorption spectrum has been calculated by including the interactions between the probe field and electrons in the QW's and between the probe and pump-laser fields.

In our numerical calculation, the laser-field absorption coefficient and refractive-index function of electrons in the resonant asymmetric double quantum wells with intersubband pumping have been studied for different laser-field strengths, momentum-dependent energy-level separations, electron tunneling, and degrees of off-resonance. The zero absorption in the overlapping region within a small tunneling gap due to quantum interference between a pair of nearly

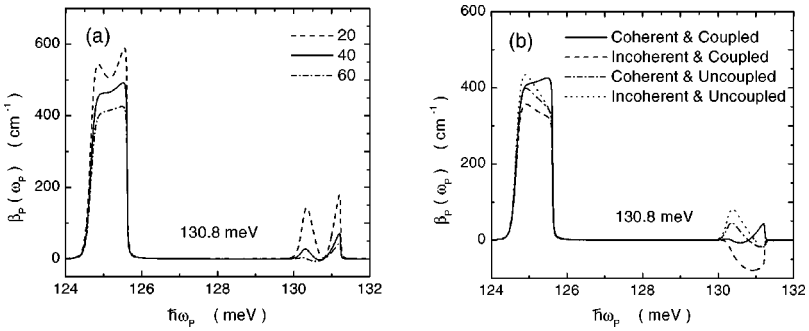

FIG. 11. $\beta_P(\omega_P)$ for the sample shown in Fig. 1(b) as a function of $\hbar\omega_P$ with $\hbar\omega_L=130.8$ meV. $\beta_P(\omega_P)$ are presented in (a) for $|\mathbf{E}_L^0|=20$, 40, and 60 kV/cm and in (b) for four different cases as defined in Fig. 10.

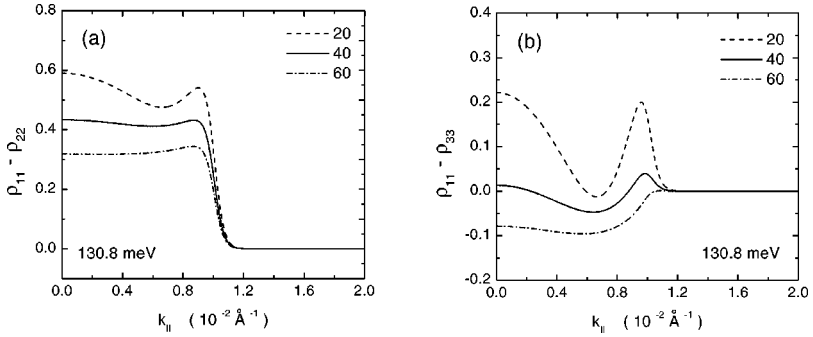

FIG. 12. $\rho_{11}(k_\parallel)-\rho_{jj}(k_\parallel)$ with $j=2,3$ for the sample shown in Fig. 1(b) as a function of $k_\parallel$ at $|\mathbf{E}_L^0|=40$ kV/cm and $\hbar\omega_L=130.8$ meV. $\rho_{11}(k_\parallel)-\rho_{22}(k_\parallel)$ and $\rho_{11}(k_\parallel)-\rho_{33}(k_\parallel)$ are, respectively, displayed in (a) and (b) for $|\mathbf{E}_L^0|=20$, 40, and 60 kV/cm.

degenerate electron transitions has been found for the pump laser and explained. The quantum interference has been clearly demonstrated through the phase cancellation between the two statistically averaged transition dipole moments. The laser frequency for the zero absorption is tunable within the tunneling gap if a small dc bias field is applied in the z direction. The momentum-dependent energy-level separation has been found to be the most predominant in destroying quantum interference in the system. For the weak probe field, we have investigated its linear absorption spectrum and refractive-index function in the same system selectively coupled by a laser field with different intensities. The optical gain of the probe field has been observed as a hole in the weak absorption peak, which has been demonstrated as a result of the partial inversion of the electron occupation probabilities in momentum space after the system is selectively pumped by a laser. The optical gain of the probe field has been found to be increasing with the pump-laser strength. The influences of the induced quantum coherence and off-diagonal radiative-decay coupling on the probe-field absorption have been quantitatively analyzed.

We make some remarks here on the simplification made in our model for RADQW's with laser pumping. The *adiabatic approximation* in Eq. (20) is subject to the *weak interaction* between the electrons and spontaneously radiated photons, which can be justified in the absence of a laser cavity. The approximation of the *long-time limit* in Eq. (21) simplifies the calculation of the matrix elements of radiative decays, which can be eliminated in principle by explicitly calculating the integral with time. The approximation for neglecting the Lamb energy shift and the imaginary part of the off-diagonal radiative-decay coupling matrix elements can be justified as long as the energy separation of different electronic states is large enough. The *rotating-wave approximation* survives only after a characteristic time, which should be eliminated when the full dynamics of electrons is studied by using the density-matrix equations [20]. Finally, if the electron density is kept low enough, as with the one used in this paper, the many-body effect has very little influence on the spectra calculated here. We have not included the electron-electron interaction in our model, which can renormalize the energy of electrons and introduce a screening to the electron-electron, electron-impurity, and electron-phonon interactions. It can be incorporated into our model by using the standardized many-body technique [20]. For modulation-doped structures with ideal interfaces at zero temperature, the scattering of electrons by impurities, roughness, and phonons is expected to be negligibly small. Moreover, the extremely fast scattering between electrons for low-density samples considered here has very little effect on the optical spectra of electrons in the steady state. The scattering between electrons and the scattering of electrons with impurities, roughness at interfaces, and phonons, which can be included in the Born approximation [21,22], are all neglected for simplicity.

APPENDIX A: EIGHT-BAND k·p DESCRIPTION OF QUANTUM WELLS

For zinc-blende-structure III-V semiconductor materials with direct band gap, the conduction- (valence-) band minima (maxima) near the Γ point ($\mathbf{k}=0$) can be well described by considering only eight bands [23], i.e., $\Gamma_6^{\pm 1/2}$, $\Gamma_8^{\pm 3/2}$, $\Gamma_8^{\pm 1/2}$, and $\Gamma_7^{\pm 1/2}$. Here, $\Gamma_6^{\pm 1/2}$ is the lowest conduction band for the up and down spins, $\Gamma_8^{\pm 3/2}$ and $\Gamma_8^{\pm 1/2}$ represent the two highest degenerate valence bands for both spin directions, and $\Gamma_7^{\pm 1/2}$ is the spin-orbit split valence band with different spins. If the wells and barriers of a QW are composed of narrow- and wide-band-gap semiconductor materials, the eight-band $\mathbf{k}\cdot\mathbf{p}$ Hamiltonian matrix can be written as [23]

$$\underline{\mathcal{H}}=\underline{\mathcal{H}}^{\mathbf{k}\cdot\mathbf{p}}+\underline{\mathcal{H}}^{\mathrm{SO}}+\underline{\mathcal{D}}^{\mathbf{k}\cdot\mathbf{p}}+\underline{\mathcal{D}}^{\mathrm{SO}}, \tag{A1}$$

where $\underline{\mathcal{H}}^{\mathbf{k}\cdot\mathbf{p}}$ includes the kinetic and potential energies of electrons and the $\mathbf{k}$-independent part of the spin-orbit interaction, $\mathcal{H}^{\mathrm{SO}}$ is the $\mathbf{k}$-dependent part of the spin-orbit interaction, $\underline{\mathcal{D}}^{\mathbf{k}\cdot\mathbf{p}}$ represents the orbital part of the strain interaction, and $\underline{\mathcal{D}}^{\mathrm{SO}}$ corresponds to the $\mathbf{k}$-independent spin-orbit part of the strain interaction. The $\mathbf{k}$-dependent spin-orbit part of the strain interaction is very small [23] and neglected here.

The first matrix $\underline{\mathcal{H}}^{\mathbf{k}\cdot\mathbf{p}}$ on the right-hand side of Eq. (A1) is given by

$$\begin{bmatrix} A & 0 & T^{\dagger}+V^{\dagger} & 0 & -\sqrt{3}(T-V) & \sqrt{2}(W-U) & W-U & \sqrt{2}(T^{\dagger}+V^{\dagger}) \\ 0 & A & \sqrt{2}(W-U) & -\sqrt{3}(T^{\dagger}+V^{\dagger}) & 0 & T-V & -\sqrt{2}(T-V) & W^{\dagger}+U^{\dagger} \\ T+V & \sqrt{2}(W^{\dagger}-U^{\dagger}) & -P+Q & -S^{\dagger} & R & 0 & (\sqrt{3/2})S & -\sqrt{2}Q \\ 0 & -\sqrt{3}(T+V) & -S & -P-Q & 0 & R & -\sqrt{2}R & (1/\sqrt{2})S \\ -\sqrt{3}(T^{\dagger}-V^{\dagger}) & 0 & R^{\dagger} & 0 & -P-Q & S^{\dagger} & (1/\sqrt{2})S^{\dagger} & \sqrt{2}R^{\dagger} \\ \sqrt{2}(W^{\dagger}-U^{\dagger}) & T^{\dagger}-V^{\dagger} & 0 & R^{\dagger} & S & -P+Q & \sqrt{2}Q & (\sqrt{3/2})S^{\dagger} \\ W^{\dagger}-U^{\dagger} & -\sqrt{2}(T^{\dagger}-V^{\dagger}) & (\sqrt{3/2})S^{\dagger} & -\sqrt{2}R^{\dagger} & (1/\sqrt{2})S & \sqrt{2}Q & Z & 0 \\ \sqrt{2}(T+V) & W+U & -\sqrt{2}Q & (1/\sqrt{2})S^{\dagger} & \sqrt{2}R & (\sqrt{3/2})S & 0 & Z \end{bmatrix}, \quad \text{(A2)}$$

where we have introduced the following notations for the matrix elements in Eq. (A2):

$$A=-(\hbar^2/2m_0)\partial/\partial z[C(z)\partial/\partial z]+E_G+U_c(z)+(\hbar^2k_{\parallel}^2/2m_0)C(z),$$

$$T+V=(k_{\parallel}/\sqrt{6})\{-(i/2)e^{i\theta}[B(z)\partial/\partial z+(\partial/\partial z)B(z)]+P_0(z)e^{-i\theta}\},$$

$$T-V=(k_{\parallel}/\sqrt{6})\{-(i/2)e^{i\theta}[B(z)\partial/\partial z+(\partial/\partial z)B(z)]-P_0(z)e^{-i\theta}\},$$

$$W+U=(i/2\sqrt{3})\{k_{\parallel}^2\sin 2\theta B(z)-[P_0(z)\partial/\partial z+(\partial/\partial z)P_0(z)]\},$$

$$W-U=(i/2\sqrt{3})\{k_{\parallel}^2\sin 2\theta B(z)+[P_0(z)\partial/\partial z+(\partial/\partial z)P_0(z)]\},$$

$$-P+Q=(\hbar^2/2m_0)\partial/\partial z\{[\gamma_1(z)+2\gamma_2(z)]\partial/\partial z\}-(\hbar^2k_{\parallel}^2/2m_0)[\gamma_1(z)-\gamma_2(z)]-U_p(z),$$

$$-P-Q=(\hbar^2/2m_0)\partial/\partial z\{[\gamma_1(z)-2\gamma_2(z)]\partial/\partial z\}-(\hbar^2k_{\parallel}^2/2m_0)[\gamma_1(z)+\gamma_2(z)]-U_p(z),$$

$$S=-i\sqrt{3}e^{-i\theta}(\hbar^2k_{\parallel}^2/2m_0)=[\gamma_3(z)\partial/\partial z+(\partial/\partial z)\gamma_3(z)],$$

$$R=-\sqrt{3}(\hbar^2k_{\parallel}^2/2m_0)\gamma_2(z)\{\cos 2\theta-i[\gamma_3(z)/\gamma_2(z)]\sin 2\theta\},$$

$$Q=(\hbar^2/m_0)\partial/\partial z[\gamma_2(z)\partial/\partial z]+(\hbar^2k_{\parallel}^2/2m_0)\gamma_2(z),$$

$$Z=(\hbar^2/2m_0)\partial/\partial z[\gamma_1'(z)\partial/\partial z]-(\hbar^2k_{\parallel}^2/2m_0)\gamma_1'(z)-U_p(z)-\Delta_0(z). \quad \text{(A3)}$$

In Eqs. (A3), m_0 is the free-electron mass, $\mathbf{k}_{\parallel}=(k_x,k_y)$ is the wave vector of electrons within the QW plane perpendicular to the z direction, θ is defined through $\mathbf{k}_{\parallel}=(k_{\parallel}\cos\theta,\ k_{\parallel}\sin\theta)$, and E_G is the band gap of the well material. $U_c(z)$ and $U_p(z)$ are the conduction- and valence-band potential profiles of the QW's, and $\Delta_0(z)$ is the spin-orbit splitting gap. The factors $C(z)$ and $\gamma_1'(z)$ represent the electron effective masses in the conduction and spin-orbit split bands. $\gamma_1(z)$, $\gamma_2(z)$, and $\gamma_3(z)$ are the modified Lüttinger parameters [23], which relate to the effective masses of heavy and light holes in the two topmost degenerate valence bands. $B(z)$ is the inversion symmetry parameter and $P_0(z)$ is the mixing parameter between the electron states in the conduction and valence bands.

The second term on the right-hand side of Eq. (A1) is found to be

$$\underline{\underline{\mathcal{H}}}^{\mathrm{SO}}=\begin{bmatrix} \underline{0} & \underline{\mathcal{T}}_1 & \underline{\mathcal{T}}_2 \\ \underline{\mathcal{T}}_1^{\dagger} & \underline{0} & \underline{0} \\ \underline{\mathcal{T}}_2^{\dagger} & \underline{0} & \underline{0} \end{bmatrix}, \quad \text{(A4)}$$

where the two submatrices in Eq. (A4) are

$$\underline{\mathcal{T}}_1=\begin{bmatrix} -[N_0(z)/\sqrt{2}]k_{\parallel}e^{i\theta} & 0 & -(\sqrt{3/2})N_0(z)k_{\parallel}e^{-i\theta} & \sqrt{2}G(z) \\ \sqrt{2}G(z) & (\sqrt{3/2})N_0(z)k_{\parallel}e^{i\theta} & 0 & [N_0(z)/\sqrt{2}]k_{\parallel}e^{-i\theta} \end{bmatrix}, \quad \text{(A5)}$$

$$\underline{\mathcal{T}}_2=\begin{bmatrix} -2G(z) & 2N_0(z)k_{\parallel}e^{i\theta} \\ 2N_0(z)k_{\parallel}e^{-i\theta} & 2G(z) \end{bmatrix}, \quad \text{(A6)}$$

with the following notation introduced in Eqs. (A5) and (A6):

$$G(z)=-\frac{i}{2}\left[N_0(z)\frac{\partial}{\partial z}+\frac{\partial}{\partial z}N_0(z)\right]. \tag{A7}$$

In Eqs. (A5)–(A7), $N_0(z)$ describes the effect of the **k**-dependent part of the spin-orbit interaction.

The third matrix $\underline{\mathcal{D}}^{\mathbf{k}\cdot\mathbf{p}}$ on the right-hand side of Eq. (A1) takes the anisotropic form of

$$\begin{bmatrix}
a'e & 0 & t^\dagger-v^\dagger & 0 & -\sqrt{3}(t+v) & \sqrt{2}(w+u) & w+u & \sqrt{2}(t^\dagger-v^\dagger)\\
0 & a'e & \sqrt{2}(w+u) & -\sqrt{3}(t^\dagger-v^\dagger) & 0 & t+v & -\sqrt{2}(t+v) & w^\dagger-u^\dagger\\
t-v & \sqrt{2}(w^\dagger+u^\dagger) & -p+q & -s^\dagger & r & 0 & (\sqrt{3/2})s & -\sqrt{2}q\\
0 & -\sqrt{3}(t-v) & -s & -p-q & 0 & r & -\sqrt{2}r & (1/\sqrt{2})s\\
-\sqrt{3}(t^\dagger+v^\dagger) & 0 & r^\dagger & 0 & -p-q & s^\dagger & (1/\sqrt{2})s^\dagger & \sqrt{2}r^\dagger\\
\sqrt{2}(w^\dagger+u^\dagger) & t^\dagger+v^\dagger & 0 & r^\dagger & s & -p+q & \sqrt{2}q & (\sqrt{3/2})s^\dagger\\
w^\dagger+u^\dagger & -\sqrt{2}(t^\dagger+v^\dagger) & (\sqrt{3/2})s^\dagger & -\sqrt{2}r^\dagger & (1/\sqrt{2})s & \sqrt{2}q & -ae & 0\\
\sqrt{2}(t-v) & w-u & -\sqrt{2}q & (1/\sqrt{2})s^\dagger & \sqrt{2}r & (\sqrt{3/2})s & 0 & -ae
\end{bmatrix}, \tag{A8}$$

where $e(z)=e_{xx}(z)+e_{yy}(z)+e_{zz}(z)$ is the trace of a strain tensor $\underline{\mathbf{e}}(z)\equiv[e_{ij}(z)]$ for $i,j=x,y,z$, and

$$t=(1/\sqrt{6})b'(z)[e_{xz}(z)+ie_{yz}(z)],$$

$$v=(1/\sqrt{6})P_0(z)\{[e_{xx}(z)-ie_{yx}(z)]k_x+[e_{xy}(z)-ie_{yy}(z)]k_y\}+g_1(z),$$

$$w=(i/\sqrt{3})b'(z)e_{xy}(z),$$

$$u=(1/\sqrt{3})P_0(z)[e_{zx}(z)k_x+e_{zy}(z)k_y]+g_2(z),$$

$$p=a(z)[e_{xx}(z)+e_{yy}(z)+e_{zz}(z)],$$

$$q=b(z)\{e_{zz}(z)-[e_{xx}(z)+e_{yy}(z)]/2\},$$

$$s=-d(z)[e_{xz}(z)-ie_{yz}(z)],$$

$$r=(\sqrt{3}/2)b(z)[e_{xx}(z)-e_{yy}(z)]-id(z)e_{xy}(z). \tag{A9}$$

In Eqs. (A9), we have defined the notations

$$g_1(z)=-\frac{i}{2\sqrt{6}}\left\{P_0(z)[e_{xz}(z)-ie_{yz}(z)]\frac{\partial}{\partial z}+\frac{\partial}{\partial z}P_0(z)[e_{xz}(z)-ie_{yz}(z)]\right\}, \tag{A10}$$

$$g_2(z)=-\frac{i}{2\sqrt{3}}\left[P_0(z)e_{zz}(z)\frac{\partial}{\partial z}+\frac{\partial}{\partial z}P_0(z)e_{zz}(z)\right]. \tag{A11}$$

$a(z)$, $b(z)$, $d(z)$, $a'(z)$, and $b'(z)$ in Eqs. (A9) include the coupling effect of electron energy bands to the strain. Among them, $a(z),b(z),d(z)$ are the Pikus-Bir deformation potential constants. The z-dependent strain tensor $[e_{ij}(z)]$ is defined by the relation $c_i(z)=c_0(z)[1+e_{ix}(z)+e_{iy}(z)+e_{iz}(z)]$ for $i=x,y,z$, where $c_i(z)$ is the anisotropic lattice constant of a layer under a strain and $c_0(z)$ is the isotropic lattice constant with no strain.

The fourth term on the right-hand side of Eq. (A1) is given by

$$\underline{\mathcal{D}}^{\mathrm{SO}}=\begin{bmatrix}\underline{0} & \underline{0} & \underline{0}\\ \underline{0} & \underline{\mathcal{D}}_1 & \underline{\mathcal{D}}_2\\ \underline{0} & \underline{\mathcal{D}}_2^\dagger & \underline{\mathcal{D}}_3\end{bmatrix}, \tag{A12}$$

where the three submatrices in Eq. (A12) are

$$\underline{\mathcal{D}}_1=\begin{bmatrix} [\Delta_0(z)/3]e & -[2\Delta_0(z)/3\sqrt{3}][e_{xz}+ie_{yz}] & i[2\Delta_0(z)/3\sqrt{3}]e_{xy} & 0 \\ -[2\Delta_0(z)/3\sqrt{3}][e_{xz}-ie_{yz}] & [\Delta_0(z)/3]e & 0 & i[2\Delta_0(z)/3\sqrt{3}]e_{xy} \\ -i[2\Delta_0(z)/3\sqrt{3}]e_{xy} & 0 & [\Delta_0(z)/3]e & [2\Delta_0(z)/3\sqrt{3}][e_{xz}+ie_{yz}] \\ 0 & -i[2\Delta_0(z)/3\sqrt{3}]e_{xy} & [2\Delta_0(z)/3\sqrt{3}][e_{xz}-ie_{yz}] & [\Delta_0(z)/3]e \end{bmatrix}, \tag{A13}$$

$$\underline{\mathcal{D}}_2=\begin{bmatrix} -[\Delta_0(z)/3][e_{xz}-ie_{yz}] & -[\Delta_0(z)/9\sqrt{2}][3e_{zz}-e] \\ [\Delta_0(z)/3\sqrt{6}][e_{xx}-e_{yy}+i2\sqrt{2}e_{xy}] & -[\Delta_0(z)/3\sqrt{3}][e_{xz}-ie_{yz}] \\ -[\Delta_0(z)/3\sqrt{3}][e_{xz}+ie_{yz}] & -[\Delta_0(z)/3\sqrt{6}][e_{xx}-e_{yy}-i2\sqrt{2}e_{xy}] \\ [\Delta_0(z)/9\sqrt{2}][3e_{zz}-e] & -[\Delta_0(z)/3][e_{xz}+ie_{yz}] \end{bmatrix}, \tag{A14}$$

$$\underline{\mathcal{D}}_3=\begin{bmatrix} -(2/3)\Delta_0(z)e(z) & 0 \\ 0 & -(2/3)\Delta_0(z)e(z) \end{bmatrix}. \tag{A15}$$

In Eqs. (A13) and (A14), we have not shown for clarity the z dependence of the strain tensor $[e_{ij}(z)]$ and its trace $e(z)=e_{xx}(z)+e_{yy}(z)+e_{zz}(z)$.

The wave function of electrons in both the conduction and valence bands of the QW's can be expanded by eight Bloch functions $u_n^B(\mathbf{r})$ with $n=1,2,\ldots,8$ corresponding to the eight different bands,

$$\psi_{j\mathbf{k}_\parallel}(\mathbf{r})=\frac{1}{\sqrt{\mathcal{S}}}e^{i\mathbf{k}_\parallel\cdot\mathbf{r}_\parallel}\sum_{n=1}^{8}F_{j\mathbf{k}_\parallel}^n(z)u_n^B[\mathbf{r}-\underline{\mathbf{e}}(z)\cdot\mathbf{r}], \tag{A16}$$

where $\mathcal{S}$ is the cross-section area of the QW's, $\mathbf{r}$ is the three-dimensional position vector, $\mathbf{r}_\parallel$ and $\mathbf{k}_\parallel$ are the two-dimensional position and wave vectors within the QW plane, and the envelope function $F_{j\mathbf{k}_\parallel}^n(z)$ in Eq. (A16) for $j=1,2,\ldots,8$ satisfies the Schrödinger equation

$$\sum_{n=1}^{8}[\mathcal{H}_{jn}-\mathcal{E}_n(\mathbf{k}_\parallel)\delta_{jn}]F_{j\mathbf{k}_\parallel}^n(z)=0, \tag{A17}$$

which is subject to the normalization condition for any integer j,

$$\sum_{n=1}^{8}\int_{-\infty}^{+\infty}dz|F_{j\mathbf{k}_\parallel}^n(z)|^2=1. \tag{A18}$$

The jth energy level of electrons with $\psi_{j\mathbf{k}_\parallel}(\mathbf{r})$ in the QW's is determined from

$$\det[\mathcal{H}_{ij}-\mathcal{E}_j(\mathbf{k}_\parallel)\delta_{ij}]=0. \tag{A19}$$

In the expansion of $\psi_{j\mathbf{k}_\parallel}(\mathbf{r})$ in Eq. (A16), $u_j^B(\mathbf{r})$ for $j=1,2,\ldots,8$ are selected as

$$\mathbf{u}^B(\mathbf{r})=\begin{bmatrix} |S\rangle\chi_\downarrow \\ |S\rangle\chi_\uparrow \\ -(i/\sqrt{6})(|X\rangle+i|Y\rangle)\chi_\downarrow+i(\sqrt{2/3})|Z\rangle\chi_\uparrow \\ (i/\sqrt{2})(|X\rangle+i|Y\rangle)\chi_\uparrow \\ -(i/\sqrt{2})(|X\rangle-i|Y\rangle)\chi_\downarrow \\ (i/\sqrt{6})(|X\rangle-i|Y\rangle)\chi_\uparrow+i(\sqrt{2/3})|Z\rangle\chi_\downarrow \\ -(i/\sqrt{3})(|X\rangle-i|Y\rangle)\chi_\uparrow+(i/\sqrt{3})|Z\rangle\chi_\downarrow \\ -(i/\sqrt{3})(|X\rangle+i|Y\rangle)\chi_\downarrow-(i/\sqrt{3})|Z\rangle\chi_\uparrow \end{bmatrix}, \tag{A20}$$

where $|S\rangle$ is the $J=0$ orbital function and $|X\rangle$, $|Y\rangle$, and $|Z\rangle$ are the three $J=1$ orbital functions with $m_J=0,\pm1$ in the angular-momentum representation $|J,m_J\rangle$. The spinors for electrons with up and down spins in Eq. (A20) are

$$\chi_\downarrow=\begin{bmatrix}0\\1\end{bmatrix},\quad \chi_\uparrow=\begin{bmatrix}1\\0\end{bmatrix}. \tag{A21}$$

[1] P. W. Milonni, Phys. Rep. C **25**, 1 (1976).
[2] D. A. Cardimona, M. G. Raymer, and C. R. Stroud, Jr., J. Phys. B **15**, 55 (1982).
[3] D. A. Cardimona, M. P. Sharma, and M. A. Ortega, J. Phys. B **22**, 4029 (1989).
[4] D. A. Cardimona, Phys. Rev. A **41**, 5016 (1990).
[5] S. E. Harris, Phys. Rev. Lett. **62**, 1033 (1989); S. E. Harris, J. E. Field, and A. Imamoğlu, *ibid.* **64**, 1107 (1990).
[6] M. O. Scully, S. Zhu, and A. Gavrielides, Phys. Rev. Lett. **62**, 2813 (1989); M. O. Scully, *ibid.* **67**, 1855 (1991).
[7] A. Imamoğlu, J. E. Field, and S. E. Harris, Phys. Rev. Lett. **66**, 1154 (1991).
[8] J. Gao, C. Guo, X. Guo, G. Jin, P. Wang, J. Zhao, H. Zhang, Y. Jiang, D. Wang, and D. Jiang, Opt. Commun. **93**, 323

(1992); A. S. Zibrov, M. D. Lukin, D. E. Nikonov, L. Hollberg, M. O. Scully, V. L. Velichansky, and H. G. Robinson, Phys. Rev. Lett. **75**, 1499 (1995).
[9] J. Faist, F. Capasso, C. Sirtori, K. W. West, and L. N. Pfeiffer, Nature (London) **390**, 589 (1997).
[10] H. Schmidt, K. L. Campman, A. C. Gossard, and A. Imamoğlu, Appl. Phys. Lett. **70**, 3455 (1997).
[11] S. M. Sadeghi, J. F. Young, and J. Meyer, Phys. Rev. B **51**, 13 349 (1995).
[12] Y. Zhao, D. H. Huang, and C. Wu, Opt. Lett. **19**, 816 (1994).
[13] A. Imamoğlu and R. J. Ram, Opt. Lett. **19**, 1744 (1994).
[14] D. S. Lee and K. J. Malloy, IEEE J. Quantum Electron. **30**, 85 (1994).
[15] A. Imamoğlu and S. E. Harris, Opt. Lett. **14**, 1344 (1989).
[16] A. L. Fetter, *Quantum Theory of Many-Particle Systems* (McGraw-Hill, Inc., New York, 1971).
[17] K. Meissner, B. Fluegel, H. Gießen, B. P. McGinnis, A. Paul, R. Binder, S. W. Koch, and N. Peyghambarian, Phys. Rev. B **48**, 15 472 (1993).
[18] D. H. Huang and M. O. Manasreh, Phys. Rev. B **54**, 5620 (1996).
[19] D. H. Huang and S. K. Lyo, Phys. Rev. B **59**, 7600 (1999).
[20] D. H. Huang and D. A. Cardimona, J. Opt. Soc. Am. B **15**, 1578 (1998).
[21] M. Lindberg and S. W. Koch, Phys. Rev. B **38**, 3342 (1988).
[22] D. H. Huang and S. K. Lyo, J. Phys.: Condens. Matter **12**, 3383 (2000).
[23] T. B. Bahder, Phys. Rev. B **41**, 11 992 (1990).